



UPPSALA
UNIVERSITET

*Digital Comprehensive Summaries of Uppsala Dissertations
from the Faculty of Science and Technology 959*

Thin Film Plate Acoustic Resonators for Frequency Control and Sensing Applications

LILIA ARAPAN



ACTA
UNIVERSITATIS
UPSALIENSIS
UPPSALA
2012

ISSN 1651-6214
ISBN 978-91-554-8437-8
urn:nbn:se:uu:diva-178592

Dissertation presented at Uppsala University to be publicly examined in Polhemsalen, Ångströmlaboratoriet, Lägerhyddsvägen 1, Uppsala, Friday, September 28, 2012 at 09:15 for the degree of Doctor of Philosophy. The examination will be conducted in English.

Abstract

Arapan, L. 2012. Thin Film Plate Acoustic Resonators for Frequency Control and Sensing Applications. Acta Universitatis Upsaliensis. *Digital Comprehensive Summaries of Uppsala Dissertations from the Faculty of Science and Technology* 959. 78 pp. Uppsala. ISBN 978-91-554-8437-8.

The recent development of the commercially viable thin film electro-acoustic technology has triggered a growing interest in the research of plate guided wave or Lamb wave components owing to their unique characteristics. In the present thesis i) an experimental study of the thin film plate resonators (FPAR) performance operating on the lowest symmetrical Lamb wave (S₀) propagating in highly textured AlN membranes versus a variety of design parameters has been performed. The S₀ mode is excited through an Interdigital Transducer and confined within the structure by means of reflection from metal strip gratings. Devices operating in the vicinity of the stop-band center exhibiting a Q-value of up to 3000 at a frequency around 900MHz have been demonstrated. Temperature compensation of this type of devices has been studied theoretically and successfully realized experimentally for the first time. Further, integrated circuit-compatible S₀ Lamb based two-port FPAR stabilized oscillators exhibiting phase noise of -92 dBc/Hz at 1 kHz frequency offset with feasible thermal noise floor below -180 dBc/Hz have been tested under high power for a couple of weeks. More specifically, the FPARs under test have been running without any performance degradation at up to 27 dBm loop power. Further, the S₀ mode was experimentally demonstrated to be highly mass and pressure sensitive as well as suitable for in-liquid operation, which together with low phase noise and high Q makes it very suitable for sensor applications; ii) research in view of FPARs operating on other types of Lamb waves as well as novel operation principles has been initiated. In this work, first results on the design, fabrication and characterization of two novel type resonators: The Zero Group Velocity Resonators (ZGVR) and The Intermode-Coupled Thin Film Plate Acoustic Resonators (IC-FPAR), exploiting new principles of operation have been successfully demonstrated. The former exploits the intrinsic zero group velocity feature of the S₁ Lamb mode for certain combination of design parameters while the latter takes advantage of the intermode interaction (involving scattering) between S₀ and A₁ Lamb modes through specially designed metal strip gratings (couplers). Thus both type of resonators operate on principles of confining energy under IDT other than reflection.

Keywords: Electro-Acoustics, FPAR, Lamb waves, aluminium nitride, interdigital transducer, phase noise, temperature compensation, power handling, sensitivity, zero group velocity, intermode coupling

Lilia Arapan, Uppsala University, Department of Engineering Sciences, Solid State Electronics, Box 534, SE-751 21 Uppsala, Sweden.

© Lilia Arapan 2012

ISSN 1651-6214

ISBN 978-91-554-8437-8

urn:nbn:se:uu:diva-178592 (<http://urn.kb.se/resolve?urn=urn:nbn:se:uu:diva-178592>)

*This thesis is dedicated to my dear mother,
Alla Mihailovna and my little angels,
Alexander and Miranda.*

List of Papers

This thesis is based on the following papers, which are referred to in the text by their Roman numerals.

- I Yantchev, V., Arapan, L., Katardjiev, I. (2009) Micromachined Thin Film Plate Acoustic Wave Resonators (FPAR): Part II *IEEE Transactions On Ultrasonics Ferroelectrics And Frequency Control* 56(12): 2701-2710
- II Wingqvist, G., Arapan, L., Yantchev, V., Katardjiev, I. (2009) A Micromachined thermally compensated thin film Lamb wave resonator for frequency control and sensing applications *J. Micromech. Microeng.* 19(3): 035018
- III Arapan, L., Avramov, I., Yantchev, V. (2011) Thin film plate acoustic resonators for integrated microwave power oscillator applications *Electronic Letters* 47(7):453-454
- IV Arapan, L., Anderas, E., Katardjiev, I., Yantchev, V. (2011) Sensitivity Features of Thin Film Plate Acoustic Wave Resonators *IEEE Sensors Journal*, 11(12): 3330-3331
- V Arapan, L., Alexieva, G., Avramov, I. D., Radeva, E., Strashilov, V., Yantchev, V., Katardjiev, I. (2011) Highly Mass-Sensitive Thin Film Plate Acoustic Resonators (FPAR) *Sensors* 11(7): 6942-6953
- VI Yantchev, V., Arapan, L., Katardjiev, I., Plessky, V. (2011) Thin-film zero-group-velocity Lamb wave resonator *Applied Physics Letters*, 99(3): 033505
- VII Arapan L., Katardjiev I., Yantchev V. (2012) An intermode-coupled thin-film micro-acoustic resonator *J. Micromech. Microeng.* 22(8): 085004

Contents

Preface	9
Author's Contribution	12
Acknowledgments	13
Abbreviations	14
Chapter 1 Background	15
1.1 Introduction to the SAW Technology	17
1.1.1 The Inter-Digital Transducer	19
1.2 Introduction to the FBAR Technology	21
1.3 The Thin Film Plate Acoustic Resonator	24
References to Chapter 1	27
Chapter 2 Microfabrication of FPAR	30
2.1 AlN Thin Film Synthesis	30
2.2 Microfabrication	31
2.3 Electrical Measurement Set-Up	33
References to Chapter 2	34
Chapter 3 Acoustic Resonators Basic Characteristics	35
3.1 Electromechanical Coupling Coefficient	35
3.2 Quality Factor of a Resonator	40
3.3 Acoustic Resonators as Sensors	41
3.3.1 Noise in Frequency and Time Domain	42
3.3.2 Sensitivity and Resolution	46
3.3.3 Thermal Stability	48
References to Chapter 3	49
Chapter 4 Summary of Included Papers	51
4.1 Paper I "Thin Film Plate Acoustic Wave Resonators (FPAR): Part II"	51
4.2 Paper II "A Micromachined Thermally Compensated Thin Film Lamb Wave Resonator for Frequency Control and Sensing Applications"	55
4.3 Paper III "Thin film plate acoustic resonators for integrated microwave power oscillator applications"	58

4.4 Paper IV “Sensitivity Features of Thin Film Plate Acoustic Wave Resonators”	60
4.5 Paper V “Highly Mass-Sensitive Thin Film Plate Acoustic Resonators (FPAR)”	62
4.6 Paper VI “Thin-film zero-group-velocity Lamb wave resonator”	68
4.7 Paper VII “An intermode-coupled thin-film micro-acoustic resonator”	70
Summary and Discussion	74
Svensk sammanfattning	76

Preface

The microwave electro-acoustics offers unique features in terms of low losses and small form factors for filter applications as well as low noise frequency sources. At the same time this technology enables fabrication of high-resolution sensors for chemical, physical or biochemical applications. Historically, the focus of the research has mainly been on the surface acoustic wave devices built on single crystal piezoelectric substrates as well as thickness excited thin film bulk acoustic waves in thin plates.

The present work is part of the research on thin film plate resonators (FPAR) that has been initiated at Uppsala University, Department of Solid State Electronics around 2004 by Dr V. Yantchev. The work in the present thesis can be divided into two main parts:

1. Experimental study of the FPAR performance employing the lowest symmetrical Lamb wave (S_0) propagating in highly textured AlN membranes versus a variety of design parameters has been performed. Devices operating in the vicinity of the stop-band center exhibiting a Q-value of up to 3000 at a frequency around 900 MHz have been demonstrated. Temperature compensation of this type of devices has been studied theoretically and successfully realized experimentally. Further, oscillators based on two-port resonators exhibited phase noise of -92 dBc/Hz at 1 kHz offset, feasibility for thermal noise floors below -180 dBm/Hz correlated to the high power handling capabilities manifested by the continuous operation for a couple of weeks at incident power levels of about 24 dBm (250 mW) without any performance degradation. The S_0 mode was proved experimentally to be highly mass and pressure sensitive as well as suitable for in-liquid operation, which together with low phase noise and high Q makes it very suitable for sensor applications.
2. The S_0 Lamb mode is the most exploited operation mode in thin film plate acoustic resonators. The acoustic energy is confined within the resonator through reflection from either an array of metal strips (distributed reflector) or from the free suspended edges of the membrane. In the second part of this thesis research in view of FPARs operating on other types of Lamb waves innovatively employing non-reflective physical principles for confining the energy within the resonator has been initiated. In this work the first results on design, fabrication and characterization of two novel type resonators, The Zero Group Veloc-

ity Resonator (ZGVR) and The Intermode-Coupled FPAR (IC-FPAR), based on the first symmetric S_1 and the first asymmetric A_1 Lamb modes has been demonstrated, respectively. Both exploit novel principles of operation. The zero group velocity resonator has been designed to work at a certain thickness-to-wavelength ratio where the S_1 Lamb mode exhibits zero group velocity which in turn promotes intrinsic self-confining of the energy. The intermode-coupled FPAR uses the refraction of the excited S_0 into the A_1 mode and back through an array of metal strips called grating coupler.

The structure of the thesis is as follows. Chapter 1 is dedicated to the introduction into electro-acoustics from historical perspectives. It also contains some general background knowledge of the field and specifically the progress in the topic before the present work has started. In Chapter 2 the topology of the FPAR is presented including micro-fabrication and electrical measurements. Chapter 3 deals with the main device characteristics such as quality factor and electromechanical coupling coefficient together with application related parameters, like sensitivity, phase noise, temperature coefficient of frequency. Brief description and discussion of the results published in the thesis papers are presented in Chapter 4.

The author of this thesis was granted the 2012 EFTF Student Award for her contributions to the topic: “Materials, Resonators and Resonator Circuits, Oscillators, Synthesisers, Noise and Circuit Technics” at the 26th European Time and Frequency Control Forum, Gothenburg, Sweden.



The 2012 EFTF Student Award

26nd EFTF, Gothenburg, 24 to 26 April 2012

Lilia Arapan

*For her contributions to the thematic:
"Materials, Resonators and Resonator Circuits,
Oscillators, Synthesisers, Noise and Circuit Techniques"*

EFTF

Bernard Dulmet
Scientific Vice-Chair

Patrick Gill
Scientific Committee Chair

Jan Johansson
Local Organisation Chair



CHALMERS



Author's Contribution

The work was carried out at the Department of Engineering Science, Solid State Electronics, Uppsala University, during 2007-2012 under supervision of Dr. V. Yantchev. In all the included papers the author has been involved to varying degree in device microfabrication, measurement and analysis of the results. In Paper I the author has not been involved only in the part concerning the Coupling of Modes analysis. Research presented in Paper II was done in collaboration with G. Wingqvist as a leading student. The author has actively participated in all stages of this development while being introduced to the needed research skills. The study in Paper III was done in collaboration with Georgy Nadjakov Institute of Solid State Physics, Bulgaria. The author actively participated in the resonators development and took full responsibility for their fabrication. The fabricated resonators were subsequently incorporated in oscillators and tested by the collaborating part. The work in Paper IV was done in collaboration with E. Anderås. The author carried out the part concerning the in-liquid measurements and evaluation. The work in Paper V was done in collaboration with Department of Solid State Physics and Microelectronics, University of Sofia, Bulgaria and Georgy Nadjakov Institute of Solid State Physics, Bulgaria. The author developed the theoretical ground of the work as well as carried out device microfabrication. The polymer coating and gas sensitivity experiments were carried out by the collaborators. In Paper VI the author was involved in part of the device microfabrication. It is noted that the other part was outsourced to VTT Finland because of the stringent technological requirements. The author performed electrical measurements as well as analysis and interpretation of the results. In Paper VII the author was involved in device design, microfabrication, measurement as well as performed 2D FEM simulations implemented in COMSOL software, forming the theoretical background of the work.

Acknowledgments

I am grateful to many people for contributing directly or indirectly in writing this thesis.

First of all I would like to express all my gratitude to my first supervisor, Dr. V. Yantchev, who introduced me into the world of Electro-Acoustics, for his continuous guidance, patience and support in all these years. Without doubts this thesis became reality only thanks to You!

I am also grateful to Prof. Ilja Katardjiev, my second supervisor, for offering me in 2007 the opportunity to work in the Division of Solid State Electronics, Uppsala University, to learn a new and exciting subject and get to know so many interesting and extraordinary people. I really appreciated Your invaluable advices related to work in general and outside it. And, of course, thank You for carefully reading this thesis and the Swedish translation!

I would like to thank all my co-authors of the papers and specially (in alphabetic order) Dr. Ivan D. Avramov from Georgy Nadjakov Institute of Solid State Physics, Bulgaria, Prof. Victor Plessky from GVR Trade SA, Switzerland and Prof. Vesseline L. Strashilov from Department of Solid State Physics and Microelectronics, University of Sofia, Bulgaria.

Many thanks go to Dr. Gunilla Wingqvist (at that time PhD student in the same division), who introduced me to the experimental part of the work, namely microfabrication and electrical measurements. I enjoyed very much the time spent outside work with You, my sister!

Now speaking about the microfabrication, many thanks to the MSL staff, and particularly to Dr. Rimantas Brukas for giving practical advices and deeper insights into the processes involved and Torvald Andersson for fighting like a hero against the notorious ICP-RIE PlasmaTherm machine.

I am thankful to Marianne Asplund for providing help and assistance in solving various bureaucratic issues.

I would like to thank my family and friends from inside the group, other groups in Ångström Laboratory and BMC as well as outside work, for the time spent together, support and long discussions about work and life in general. Special thanks in this context to Sergiu Arapan and Moreno Marcellini for their help and support.

To the reader: I suppose You will find in this thesis errors, omissions and probably over-simplifications, for which I take absolute responsibility, but I hope the reading will prove to be useful, interesting and enjoyable for You!

Abbreviations

BAW	Bulk Acoustic Wave
BGS	Bleustein-Gulyaev-Shimizu Wave
EA	Electro-Acoustics
FBAR	Thin Film Bulk Acoustic Resonator
FPAR	Thin Film Plate Acoustic Resonator
IC	Integrated Circuit
IC-FPAR	Intermode Coupled Thin Film Plate Acoustic Resonator
IDT	Interdigital Transducer
LFE	Lateral Field Excitation
LW-LFE	Longitudinal Wave Lateral Field Excitation
LSAW	Leaky Surface Acoustic Wave
RF	Radio Frequency
RSAW	Rayleigh Surface Acoustic Wave
SAW	Surface Acoustic Wave
SH	Shear Horizontal
SHAPM	Shear Horizontal Acoustic Plate Mode
SMR	Solidly Mounted Resonator
SNR	Signal to Noise Ratio
SSB	Single-Side Band
STW	Surface Transverse Wave
TCF	Temperature Coefficient of Frequency
TE	Thickness Excitation
ZGVR	Zero Group Velocity Resonator

Chapter 1 Background

Historically the focus of the research in Electro-Acoustics (EA) was on radar applications for military purposes (World War II). At that time the main requirement on the design of devices was the highest performance with less focus on price and mass manufacturability. With the transition from military applications to the commercial and customer sector, the requirements imposed on the design shifted dramatically towards the mass production at low cost while keeping an acceptable performance. Today's commercially available Radio frequency (RF) devices are based on two competing technologies, namely The Surface and Bulk Acoustic Wave resonators, SAW and BAW, respectively. Both of them use piezoelectric materials and metal electrodes as transducers to convert electrical energy into mechanical and vice versa, while employing different types of acoustic waves in solids. As the name suggests, SAW resonators take advantage of surface acoustic waves propagating on the surface of the material while BAW resonators employ bulk acoustic waves propagating in the thickness of the plate bulk. Compared to other available technologies (dielectric and waveguide resonators), acoustic wave based resonators have several advantages. The size of the resonators is usually related to the wavelength, which in turn is directly proportional to velocity and inversely proportional to frequency, $\lambda = V/f$. This means that for the same frequency of operation, acoustic resonators are much smaller in size because the acoustic wave velocity is four to five orders of magnitude lower than the velocity of electromagnetic waves. Both SAW and BAW resonators demonstrate high quality factors resulting in good energy storage and propagation. This originates from the fact that acoustic waves in crystalline materials propagate with very low losses. Another advantage is that acoustic resonators can be mass-produced by using the already well-established semiconductor technologies. This includes thin film deposition, photolithography, and manufacturability on wafer level. Last but not least the acoustic waves can be easily and conveniently excited and converted back to electrical signal by means of transducers through the piezoelectric property of SAW and BAW materials. All these resulted in miniature, low cost, and high performance devices.

The transition to acoustic wave devices has triggered an exponential growth of the wireless communication applications (including cell phones and broadband applications) in the last 40 years. For example, in 2006 the manufactured volume of SAW filters exceeded 5 billion units. Generally, most of the wireless market is occupied by SAW devices simply because it is a quite mature

technology and its manufacturing process is optimized to push the price to its lowest limit. But it is limited when it comes to frequency of operation (up to 2.5 GHz) by technological reasons that will be discussed later on. Another disadvantage of SAW devices is that they are not Integrated Circuit (IC) compatible due to materials (single crystal) they are built on, typically SiO_2 (quartz), LiTaO_3 (lithium tantalate) or LiNbO_3 (lithium niobate). On the other hand BAW resonators have been in use in electronics for many years, even before the SAW technology was developed, as notably quartz resonators and delay lines. But the upper frequency limit for a typical quartz crystal is limited by its thickness. In order to use the same principle of operation in the gigahertz range the thickness of the piezoelectric layer must be in the order of micrometers.

In recent years, thin piezoelectric films have been developed to extend the EA technology into much higher frequencies in addition to making it IC compatible. In Europe, the thin film electro-acoustic technology has been developed at a number of research centers as follows, in no specific order:

- at Uppsala University, Sweden by Prof. I. Katardjiev [1],
- at Philips Research by H. Loebl [2],
- at EPFL, Switzerland by Prof. P. Muralt [3],
- at the University Politechnic de Madrid by Prof. E. Iborra [4],
- at the Institute of Acoustics CNR, Rome by Prof. E. Verona [5],
- at VTT, Finland by Dr. T. Pensala [6].

The Thin Film Bulk Acoustic Resonator (FBAR) is a high frequency analog of the conventional bulk acoustic wave, BAW resonator. In its simplest configuration the BAW resonator is represented by a piezoelectric slab of given thickness and two electrodes deposited on either side of the slab or its counter part the solidly mounted resonator (SMR), a more mechanically rugged structure, represented by a piezoelectric thin film sandwiched between two thin electrodes and is fabricated on top of a distributed acoustic mirror to isolate the SMR from the substrate. Their fundamental drawback is sensitivity of the frequency to the technological fluctuations, but at the same time they are IC compatible (the piezo-layer usually is AlN grown on silicon), and exhibit a high power handling capability. Usually, FBARs have higher quality factors Q due to lower losses as compared to SAW devices.

The research in the field of electro-acoustics is in continuous progress. New applications put new requirements on device performance leading to new solutions. Moreover, new devices can introduce higher versatility and lead to novel applications. As a result of recent research a new type of acoustic resonators has emerged, The Thin Film *Plate* Acoustic Resonator (FPAR), employing another type of acoustic waves, Lamb waves, which are known as a class of guided waves in plates with free boundaries. The FPAR approach combines

the operation principles of SAW resonators with the technological platform of FBARs, which makes possible building devices that enjoy the advantages of both technologies: easy to fabricate, IC compatible, with high Q factors at high frequency of operation.

1.1 Introduction to the SAW Technology

The history of SAW devices has its origins back in 1885 when Lord Rayleigh for the first time reported on the existence of a slow wave propagating along the surface of an isotropic solid and explained some seismic signals arriving later after the expected ones [7]. This wave has the polarization in the sagittal plane and its amplitude vanishes exponentially in the bulk. Other geophysicists with interest in seismology extended the research. In 1911 Love has published a treatise where a shear horizontal (SH) surface wave propagating in a half space covered by a thin layer of material with a lower shear bulk velocity was described [8]. Later Sezawa demonstrated that a Rayleigh-type wave is possible also in layered structures [9]. Another crucial discovery that led to the application of acoustic waves in electronics was the direct (and later inverse) piezoelectric effect in 1880 by brothers Curie [10]. In 1968-1969 Bleustein, Gulyaev and Shimizu, independently, demonstrated the existence of another type of SH surface wave in anisotropic media, called BGS, localized close to the surface due to strong piezoelectricity in certain cuts of materials, for example in a hexagonal crystal with propagation along x direction [11, 12, 13]. When a horizontally polarized piezoactive wave (one that generates electrical fields) is propagating in a strong piezoelectric media it creates stresses near surface due to discontinuity in the electric field inside the material and outside in the vacuum. To compensate for these stresses the wave amplitude becomes non-uniform and a bulk wave transforms into a surface wave. Though this wave has an acoustic velocity higher than the slow shear bulk wave (sagittal plane polarization) they do not couple to each other due to high symmetry.

In the 1960s there were 24 different methods to generate Rayleigh waves [14], among them the wedge and the comb transducers. Both had similar principle of operation: the generated bulk wave by a piezoelectric plate transducer subsequently converted into Rayleigh wave. Preceded by a vast research towards the pulse compression radar, the idea of having a planar transducer to generate directly the surface acoustic wave was suggested independently by Rowen and Mortley in two patents from 1963 [15, 16]. The first SAW device was experimentally realized in 1965 by White and Voltmer [17]. It was a uniform *interdigital transducer* (IDT) consisting of interleaved metal electrodes on a crystal quartz substrate, generating and receiving Rayleigh waves through the direct and inverse piezoelectric effect.

The fabrication of SAW devices was relatively simple, since it was using manufacturing processes already established by the semiconductor technology, like metal deposition and, most important, lithographic techniques. At that time it was already understood that a large variety of functions could be obtained just by varying the shape of structures on the surface of substrates. For example, it was known that IDTs suffer from internal reflections by the electrodes causing unwanted signals in the frequency response. Thus, around 1972 the split-electrode-type IDT was introduced to overcome this deficiency [18, 19]. Another issue is that the IDTs generate waves in both directions, which leads to losses in their efficiency. That is why a series of different transducer configurations were established to make the IDTs unidirectional [20]. On the other hand, by placing metal gratings to act as reflectors on both sides of a bidirectional IDT one could also confine the energy and thus build a resonator. In Fig. 1.1 the topology of a typical SAW resonator is shown.

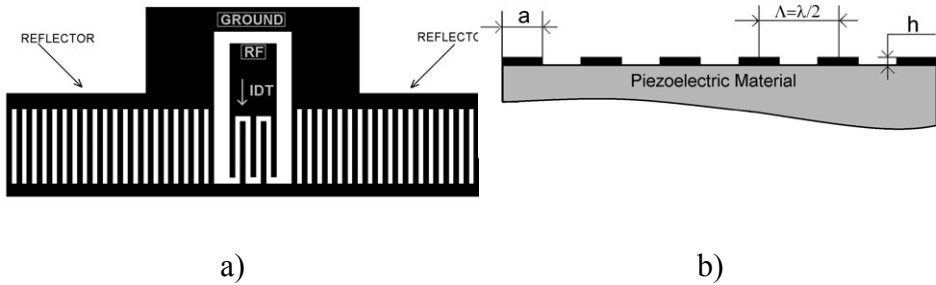


Figure 1.1 a) Top and b) side view of a typical SAW resonator.

Around 1969, Tancrrell *et al* [21] published a paper on the experimental results for a dispersive IDT SAW device on a lithium niobate substrate, and also suggested that the electrode overlaps can be varied, a technic later called “apodization”. This was the beginning of a new era in electro-acoustics.

In the late 1980s and beginning of 1990s new applications such as mobile and cordless phones required low-loss RF filters, demands, which Rayleigh waves could not meet for two main reasons. Firstly, their strong surface confinement makes them sensitive to the surface imperfections which in turn promotes larger propagation losses at higher frequencies. Secondly, the bandwidth requirements impose the employment of low loss piezoelectric waves with relatively high piezoelectric couplings, which criterion is difficult to meet for classical Rayleigh SAWs. A way to overcome these limitations was to take advantage of SH surface waves (polarization parallel to the surface). Most generally these waves are localized near the surface either by some kind of slowing-down technique or they propagate with small losses in the bulk owing to the crystal anisotropy, respectively. A remarkable example for the first type of SH-waves is represented by the *surface transverse wave* (STW) described

theoretically by Auld *et al* [22] in 1976 and Victor Plessky [23] and practically employed almost 10 years later by C. Flory and R. Bayer in their work on STW resonator design from 1987 [24]. STW is a shear horizontal wave confined to the surface by corrugating it (making the surface “slower” through grooves or gratings). Another possibility to slow-down the SH wave near the surface is to deposit on top of it a thin layer of low acoustic impedance material, resulting in a Love wave.

Though the BGS wave seems quite attractive for filter applications (no dispersion, total reflection by the crystal border, strong piezoelectric coupling and deeper localization depth than Rayleigh wave), the crystals of practical use such as quartz, LiNbO_3 or LiTaO_3 have no such cut where BGS could propagate. Alternatively, the Leaky SAW (LSAW) is similar to BGS wave, but due to the lack of symmetry a small coupling to the slow shear bulk wave can appear. In principle since it has higher velocity than the latter it should leak into the bulk, but due to either symmetry or lucky combination of constants this coupling is small or even negligible in some crystal cuts. Examples of such crystal cuts are $36\text{--}42^\circ$ LiTaO_3 or 64° LiNbO_3 . Leaky SAW have high velocities (higher than other SAWs), low losses and strong electromechanical couplings, which make them very attractive not only in military, industrial and consumer electronics but also as sensors in liquids. The majority of RF SAW filters for mobile phones employ leaky waves. Recently the temperature compensation was also realized [25].

Generally, surface acoustic waves in piezoelectrics can be classified in three main groups: Rayleigh waves, SH waves (comprising Love wave, BGS wave and STW discussed above) and leaky surface acoustic wave (LSAW), although shear LSAWs have been described above, longitudinal LSAWs also exist.

When sputtering of thin piezoelectric films became reality it was possible to go even higher in SAW velocity (frequency) by using layered structures. A thin piezoelectric film of AlN or ZnO deposited on a high velocity substrate like diamond and sapphire, together with IDT employed as transducer have been used as High Velocity SAW (HVS AW) platforms. The main drawback of this type of SAW is that they suffer from relatively large dispersion and improved losses due to the imperfections at the interface piezoelectric/substrate.

1.1.1 The Inter-Digital Transducer

The basic elements of any SAW resonator are the inter-digital transducers for generation and detection of the wave, and gratings or distributed reflectors for confining it. An IDT consists of two sets of electrodes connected alternatively to two bus bars placed on a piezoelectric substrate. Each period of an IDT consists of multiple strips. The space Λ between two adjacent electrode fingers and their overlap W are called pitch and aperture, respectively. In its simplest

form both the pitch and aperture are constant. Most often the width of the electrodes and the distance between them are equal, so that the metallization ratio is 0.5.

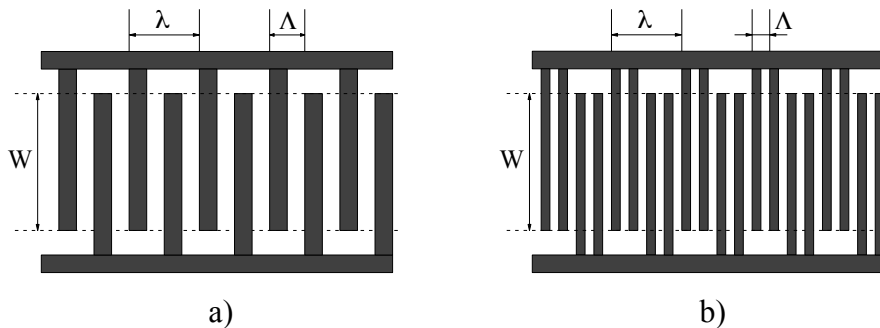


Figure 1.2 IDT topology: a) single electrode IDT and b) split electrode IDT configurations.

In Fig. 1.2 two types of IDT are presented. In configuration from Fig 1.2a the IDT consists of two strips per period, called single-electrode-type IDT, while in Fig. 1.2b there are four electrodes per period and such a configuration is called split-electrode-type IDT. One period λ is the distance between two electrodes of same polarity.

When a voltage U is applied across the electrodes an electric field is produced which generates strains propagating in both directions (Fig. 1.3). Thus various surface waves are generated by means of the inverse piezoelectric effect.

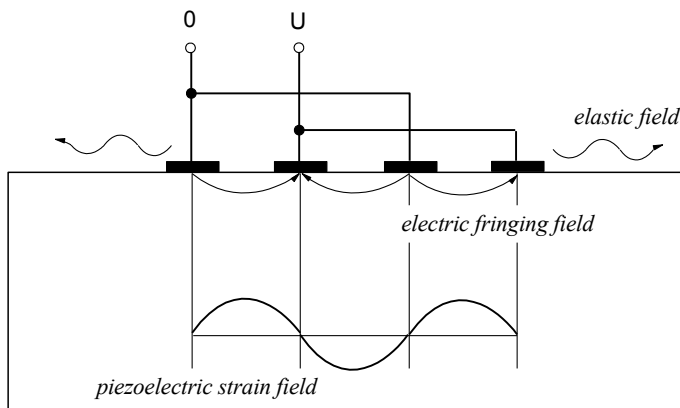


Figure 1.3 The IDT operating principle.

When the supply voltage is sinusoidal, vibrations add constructively if the periodicity of the electrodes equals the wavelength of the excited wave,

$\lambda = \lambda_0$. Gratings placed on both sides of the transducer, having the same pitch and metallization ratio as the IDT, confine the wave and form an acoustic resonator. The fundamental resonance frequency depends on the velocity of the acoustic wave and its central wavelength as $f_0 = V/\lambda_0$. This relation has two consequences. Firstly, the resonance frequency of a SAW resonator is determined by the design of the IDT. Thus, having higher operation frequencies means thinner electrodes in the transducer, which is limited by the lithographic resolution. Secondly, by employing SAW with higher velocities one can obtain higher operation frequencies for the same lithography.

The single-electrode-type IDT is widely used because of its relatively wide finger width ($\lambda/4$) in contrast to the split-electrode-type ($\lambda/8$) from the point of view of the lithographic definition. On the other hand, the mechanical reflection of such a transducer is similar to the reflection of a grating with pitch $\lambda_0/2$ and Bragg reflections occur when periodicity equals λ_0 . In applications where frequency response must be controlled precisely the second type of IDT is employed. In the split-electrode geometry the mechanical reflection of the IDT is similar to the reflection from a grating with pitch $\lambda_0/4$ and so it is suppressed at the SAW resonance frequency.

1.2 Introduction to the FBAR Technology

The thin film bulk acoustic wave technology is much younger compared to 40 years of surface acoustic waves (although the first application of BAW in electronics was the well-known quartz resonator since the World War I).

Most generally there have been four types of BAW resonator topologies and represent a piezoelectric substrate (single crystal) sandwiched between two metal plates, which can be in contact or close proximity to the substrate [26].

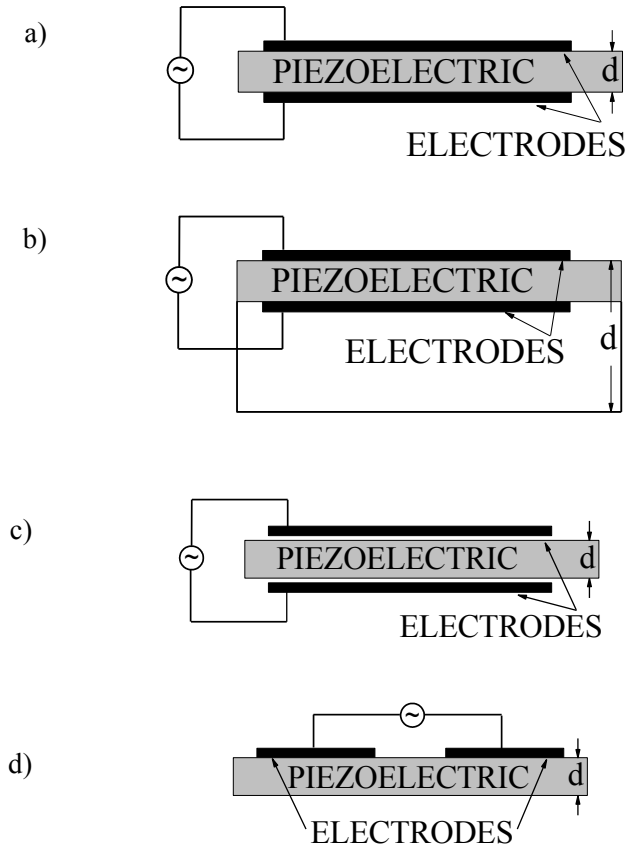


Figure 1.4 Different types of BAW resonators: a) the piezoelectric substrate (single crystal) is sandwiched between two electrode plates; b) the piezoelectric substrate between two electrode plates is situated on top of a non-piezoelectric material (overmoded resonator, OMR); c) the piezoelectric is separated by an air gap from the electrodes; d) both electrodes are on the same side of the piezoelectric substrate (lateral field excitation).

In Fig 1.4c there is a small air gap between electrodes and piezoelectric to ensure that most of the voltage is applied to the piezoelectric plate. Before 1950s this was the most typical topology of quartz resonators, but regain interest again where too thin electrodes have too much electrical loss.

The resonator in Fig. 1.4b represents a piezoelectric transducer on top of another plate of material. These resonators are called overmoded (OMR), because the acoustic path comprises multiples of half-wavelength and were used in delay line applications.

Resonators in Fig. 1.4a, b and c are so called thickness excited (TE) resonators because the acoustic wave is excited by the vertical component of the electric field, *i.e.* the wave vector and the electric field are parallel to each

other. The acoustic wave can be excited also by the orthogonal component of the fringing electric field such as in a lateral field excited resonator (LFE) represented in Fig 1.4d. The purpose of such a design is to keep the metal electrodes out of the mechanical resonance and together with the air gap coupled resonators have modern application in quartz resonators for low aging applications.

With an increased demand for higher frequencies the production of the SAW resonators have gradually increased.

Although it was clear that using single crystals for high frequency application is not technologically possible due to the fact that the resonance frequency depends on the thickness of the substrate which cannot be thinned below a certain thickness without mechanical damages and at a great cost, it was not until the development of sputtering technic of thin piezoelectric films that the interest in BAW entered a new stage. The first demonstration of a free-standing membrane FBAR was in 1980 by Grudkovskii *et al* [27] and Nakamura *et al* [28]. In 1982 was published a review paper by Lakin *et al* from TFR Technologies [29] where the future potential of FBAR was discussed, with emphasize on size reduction. The first application of FBARs was filters and the enormous contribution to this at different research centers resulted in a classic book by Rosenbaum in 1988 [30].

The piezoelectric material of choice in the first generation FBARs was ZnO, but in 1981 Lakin and Wang [31] introduced AlN as an alternative. Even if the electromechanical coupling of the first AlN sputtered films was poor it has been seen as a good choice for the future integration with IC facility, where ZnO was not welcome for its volatility and contamination issues.

Thin film bulk acoustic wave resonators consist of a piezoelectric transducer, that is a piezoelectric plate and two parallel metal plates, and the energy is confined within the resonator by the large difference in impedance at the solid/air interface (Fig. 1.5a). But there is another possibility of confining the energy: on one side the solid/air interface and using a Bragg mirror on the other side (Fig. 1.5b).

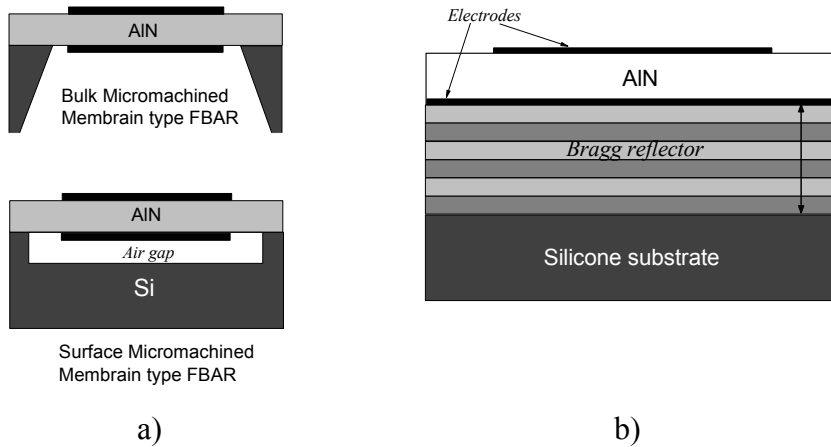


Figure 1.5 a) FBAR and b) SMR topologies.

These are called solidly mounted resonators (SMR) and were described by K. Lakin in his paper from 1995 [32]. The Bragg mirror consists of periodical repetition of a pair of films quarter thick with alternating high/low impedances, to ensure the reflection. This type of structure was very attractive due to its durability compared to free-standing membrane which in the beginning was plagued by cracks. Nevertheless the FBAR is the preferred choice for the filters because they confine better the energy and the coupling between electrical and mechanical energy is higher, parameters crucial for filter design.

Besides the standing waves in the thickness direction, laterally propagating acoustic waves are also excited in thin film resonators. These spurious resonances are guided plate or Lamb modes [33, 34], constructively reflected by the abrupt borders of the resonator electrodes. One way to suppress these spurious resonances is to design the active area of the resonator, represented by the electrodes, to have non-symmetric shapes, a technique also called apodization.

In 1997 HP Labs demonstrated a 5.2 GHz filter [35] and shortly after, the first duplexer for cell phones based on FBAR was presented by Ruby *et al* at HP Labs [36]. In early 2000s they have successfully entered the market and are produced in increased volumes.

1.3 The Thin Film Plate Acoustic Resonator

To further extend the versatility as well as functionality of thin film acoustic resonators the efforts in recent years have been directed towards the development of new types of resonators utilizing Lamb waves.

It has already been mentioned that these are guided waves laterally propagating in plates of finite thickness and have been identified as spurious resonances in thin film bulk resonators [37]. Generally, depending on the direction of particle displacement there are two different types of guided waves possible in plates, namely shear horizontal acoustic plate modes (SHAPM) and Lamb waves. The former corresponds to the horizontal polarization in the plane of the plate (shear or quasi-shear) while the latter has elliptical polarization in the sagittal plane. Generally, depending on the thickness-to-wavelength ratio the plate can support a number of these waves. Further, each type of plate modes can be classified as symmetric or antisymmetric indicating the symmetry of particle displacement relative to the median plane of the plate (Fig. 1.6a).

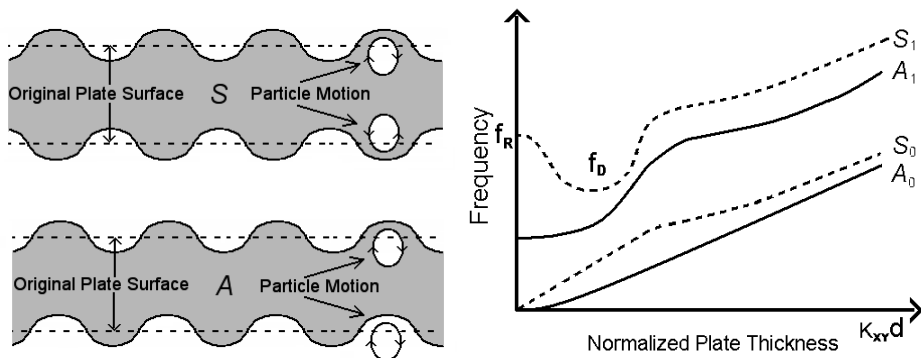


Figure 1.6 a) Lamb waves polarization (symmetric, antisymmetric); b) Dispersion curves.

From the dispersion curves (Fig. 1.6b) it is seen that Lamb waves are quite dispersive, but for a certain thickness-to-wavelength ratio the lowest symmetrical mode S_0 is low dispersive. Further, the A_0 mode seems to be suitable for low frequency applications. For semi-infinite plates the lowest A_0 and S_0 Lamb modes converge to Rayleigh wave propagating along the free surface. Note that apart from the lowest Lamb modes (A_0 and S_0) all the others have a characteristic cut-off frequency, meaning that for the lateral wave number equal to zero the mode exists and is one of the resonant plate bulk modes. For example, the first symmetric S_1 mode originates from the thickness excited (TE) longitudinal bulk mode and the A_1 mode originates from the shear bulk resonance. At frequencies slightly below the resonance frequency of the FBAR resonators, f_R , the S_1 mode starts to propagate giving rise to spurious resonances. Below the lowest allowed frequency f_D S_1 is non-propagating and spurious lateral modes are mostly represented by the lower order Lamb modes A_0 , S_0 and A_1 . Another interesting feature of the S_1 mode is its negative and zero group velocity ($V_g = d\omega/dk$) in a certain range of thickness-to-wavelength ratio, which could be exploited in RF applications.

Normally, Lamb waves were used in delay lines [38, 39] and resonators [40]. For example, the application of Lamb waves to ultrasonic delay lines was seen as a possibility to manufacture a thin delay element. In 1973 K. Toda [38] reported on Lamb wave based delay lines on lead zirconate titanate (PZT) ceramic operating on S_0 Lamb mode excited with IDT. Fabricated devices operated at 1-2 MHz and had a thickness of 0.3-0.6 mm. In his paper from 1980 M. Papalardo [39] reported on variable delay lines operating at 800 kHz (higher frequencies require thinner plates and at that time they were not commercially available). In addition, Lamb wave devices also have been used in a variety of sensors, for instance in gravimetry or for measurement of pressure or viscoelasticity [41, 42]. Substantial efforts were put in recent decades into the development of commercial plate wave based applications, but with a rather limited success. Most generally, the plates were fabricated by polishing or deep etching special cuts of expensive single crystals. Thus, despite their excellent characteristic and obvious potential, a limited number of applications could be found due to low frequency of operation, high costs and inconveniently large size.

From the technological point of view FBARs paved the way for the development of Lamb wave based electro-acoustic devices and thus the research has been reinitiated around 2005 simultaneously in Europe [37, 43] and USA [44]. Extensive studies on the lowest order symmetric Lamb wave S_0 [1, 44, 45] in c-textured AlN thin film free-standing membranes and on the first order antisymmetric Lamb wave A_1 [46] in LiNbO₃ thin film membranes have recently been performed. It has been demonstrated that Lamb waves in plates can be excited in the same way as SAW, by interdigital transducers, but the energy can be confined in the resonator in two ways: by placing reflective gratings on both sides of the IDT or it can be reflected by the suspended edges of the membrane. In the second approach, the name of “contour-mode resonator” is adopted by some authors [44] in contrast to Lamb wave resonator [45]. At the same time, fabrication of plate mode resonators similar to SMR has been reported [47]. They comprise a thin piezoelectric film deposited on top of a Bragg acoustic mirror, in which a plate wave exhibiting similar to Lamb wave behavior propagates, while enjoys the benefit of a solidly mounted structure.

The present work is dedicated to the design device optimization of thin AlN film plate resonators operating on S_0 mode, using reflective metal gratings for confining the energy, and successfully implemented in various applications: temperature compensated devices, sensors (mass, pressure, in-liquid), low noise high power oscillators, etc. Moreover, novel type of energy confinement in resonators operating on other Lamb modes (S_1 and A_1) has been proposed and experimentally demonstrated.

References to Chapter 1

1. V.Yantchev and I.Katardjiev, Micromachined thin film plate acoustic resonators utilizing the lowest order symmetric Lamb wave mode, *IEEE Trans. Ultrason. Ferroelectr. Freq. Control* **54**, 87–95 (2007)
2. H.P.Loeb1, M.Klee, C.Metzmacher, W.Brand, R.Milsom, P.Lok, Piezoelectric thin AlN films for bulk acoustic wave (BAW) resonators, *Materials Chemistry and Physics*, **79** (2–3), 143-146 (2003)
3. F.Martin, P.Muralt, M.-A.Dubois, A.Pezous, Thickness dependence of the properties of highly c-axis textured AlN thin films, *J. Vac. Sci. Technol. A*, **22**, 361-365 (2004)
4. M.Clement, E.Iborra, J.Sangrador, A.Sanz-Hervas, L.Vergara, and M.Aguila, Influence of sputtering mechanisms on the preferred orientation of aluminum nitride thin films, *Journal of Applied Physics* **94**, 1495 (2003)
5. M.Benetti, D.Cannatà, F.Di Pietrantonio, E.Verona, A.Generosi, B. Paci, and V.Rossi Albertini, Growth and characterization of piezoelectric AlN thin films for diamond-based surface acoustic wave devices, *Thin Solid Films* **497**, 304-308 (2006)
6. T.Pensala, Thin Film Bulk Acoustic Wave Devices Performance Optimization and Modeling, VTT PUBLICATIONS 756, PhD thesis (2011)
7. Lord Rayleigh, On waves propagating along the plane surface of an elastic solid, *Proc. London Math. Soc.* **17**, 4-11 (1885)
8. A.E.H.Love, Some Problems of Geodynamics. Cambridge (1911); Dover (1967)
9. K.Sezawa, Dispersion of elastic waves propagated on the surface of stratified bodies and on curved surfaces, *Bull. Earthquake Res. Inst. Tokyo*, **3**, 1-18 (1927)
10. J.Curie and P.Curie, Développement par pression de l'électricité polaire dans des cristaux hémihédriques à faces inclinées, *C. R. Acad. Sci. Paris*, **91**, 294-295 (1880)
11. J.L.Bleustein, A new surface wave in piezoelectric crystals, *Appl. Phys. Lett.*, **13**, 412-413 (1968)
12. Y.V.Gulyaev, Electroacoustic surface waves in Solids, *Soviet Phys. JETP Lett.*, **9**, 37-38 (1969)
13. Y.Ohta, K.Nakamura and H.Shimizu *Tech. Rep. IECE Japan*, vol. US69-3 (1969) (in Japanese)
14. R.M.White, Surface elastic waves, *Proc. IEEE*, **58**, 1238-1276 (1970)
15. J.H.Rowen, U.S. Patent 3,289,114 (1963)
16. W.S.Mortley, British patent 988, 102 (1963)
17. R.M.White and F.W.Voltmer, Direct piezoelectric coupling to surface elastic waves, *Appl. Phys. Lett.* **7**, 314-316 (1965)

18. A.DeVries, R.Miller and T.Wojcik, Reflection of a surface wave from three types of ID Transducer, *Proc. IEEE Ultrasonic Symp.*, 353-358 (1972)
19. T.Bristol *et al.*, Applications of double electrodes in SAW device design, *Proc. IEEE Ultrasonic Symp.*, 377-380 (1972)
20. C.S.Hartman, W.S.Jones and H.Vollers, Wideband unidirectional interdigital surface wave transducers, *IEEE UFFC Transactions*, 378-381 (1972)
21. R.H.Tancrell, M.B.Schulz, H.H.Barett, L.Davies and M.G.Holland, Dispersive delay lines using ultrasonic surface waves, *Proc. IEEE*, **57**, 1211-1213 (1969)
22. B.A.Auld, J.J.Gagnepain and M.Tan, Horizontal shear surface waves in corrugated surfaces, *Electronics Lett.*, **12**, 650-651 (1976)
23. Yu.Gulyaev and V.Plessky, "Slow" acoustic surface waves in solids, *Sov. Tech. Phys. Lett.*, **3**, 220-223 (1977)
24. C.Flory and R.Bayer, Surface Transverse Wave mode analysis and coupling to the interdigital transducers, *Proc. IEEE Ultrasonic Symp.*, 313-318 (1987)
25. K.Yamanouchi and T.Ishii, Low-Loss Wide-Band Floating Electrode Type Unidirectional Transducer Filters and Ladder-Type Resonator Filters Using High-Temperature-Stable High Electromechanical Coupling Surface Acoustic Wave Substrates, *Jpn. J. Appl. Phys.* **42**, 3166-3169 (2003)
26. K.Lakin *in* RF Bulk Acoustic Wave Filters for Communications by K.Hashimoto editor, Norwood, MA: Artech House, 2009
27. T.Grudkowski, et al. Fundamental-Mode VHF/UHF Miniature Acoustic Resonators and Filters on Silicon, *Appl. Phys. Lett.*, **37**, 993-995 (1980)
28. K.Nakamura, H.Sasaki and H.Shimizu, A piezoelectric composite resonator consisting of a ZnO film on an anisotropically etched silicon substrate, *Proc. Of 1st Symp. on Ultrason. Electronics*, Tokyo (1980)
29. K.M.Lakin et al., Thin film resonators and filters, *IEEE Ultrasonic Symposium*, 466-475 (1982)
30. J.F.Rosenbaum "Bulk acoustic Wave Theory and Devices", Norwood, MA: Artech House (1988)
31. J.Wang and K.M.Lakin, Sputtered AlN films for bulk acoustic wave devices, *IEEE Ultrasonic Symposium*, 502-507 (1981)
32. K.M.Lakin, K.T.McCarron and R.E.Rose, Solidly mounted resonators and filters, *IEEE Ultrasonics Symp.*, 905-908 (1995)
33. I.Viktorov, Rayleigh and Lamb Waves. New York: Plenum, 1967
34. B.Auld, Acoustic Fields and Waves in Solids. vol. II, New York: Wiley, 1973
35. J.Larson, R.Ruby, P.Bradley, Bulk acoustic wave resonator with improved lateral mode suppression, # 6215375 (Patent, 1999)

36. R.Ruby, P.Bradley, J.D.Larson III and Y.Oshmyansky, PCS 1900 MHz duplexers using thin film bulk acoustic resonators (FBARs), *Electronic Letters*, 35(10) (1999)
37. J. Bjurström, I. Katardjiev, and V. Yantchev, Lateral-fieldexcited thin-film Lamb wave resonator, *Appl. Phys. Lett.* **86**, 154103 (2005)
38. K.Toda, Lamb wave delay lines with interdigital electrodes, *J. Appl. Phys.*, **44**, 56–62 (1973)
39. M.Pappalardo, Stiffness-controlled variable-acoustic-delay line, *Appl. Phys. Lett.*, **37**, 893–895 (1980)
40. T.Pastureaud, W.Daniau, V.Laude, M.Wilm, Y.Malecamp and S.Ballandras, Characterization and prediction of transverse plate resonators built using mixed strip and groove gratings, in *Proc. IEEE Ultrason. Symp.*, 93–96 (2001)
41. M.F.Lewis, High frequency acoustic plate mode device employing interdigital transducers, *Electron. Lett.*, **21**, 819-821 (1981)
42. S.Ballandras, E.Gavignet, E.Bigler and G.Martin, Experimental measurements of STW properties on quartz plates of finite thickness, *Electron. Lett.* **32** (4), 414-415 (1996)
43. A.Volatie, G.Caruyer, D.P.Tanon, P.Ancey, E.Defay, B.Dubus, UHF/VHF resonators using lamb waves co-integrated with bulk acoustic wave resonators, *IEEE Ultrasonics Symposium* **2**, 902- 905 (2005)
44. G.Piazza, P.J.Stephanou, and A.P.Pisano, Piezoelectric aluminum nitride vibrating contour-mode MEMS resonators, *J. Microelectromech. Syst.* **15**, 1406 (2006)
45. C.-M.Lin, T.-T.Yen, V.V.Felmetsger, M.A.Hopcroft, J.H.Kuypers, and A.P.Pisano, Thermally compensated Aluminum Nitride Lamb wave resonators for high temperature applications, *Appl. Phys. Lett.* **97**, 083501 (2010)
46. M.Kadota, T.Ogami, K.Yamamoto, and H.Tochishita, LiNbO₃ thin film for A₁ mode of Lamb wave resonators, *Phys. Status Solidi A* **208**, 1068 (2011)
47. I.Kone, F.Domingue, A.Reinhardt, H.Jacquinet, M.Borel, M.Gorisse, G.Parat, F.Casset, D.Pellissier-Tanon, J.F.Carpentier, L.Buchaillot and B.Dubus, Guided acoustic wave resonators using an acoustic Bragg mirror, *Appl. Phys. Lett.* **96**, 223504 (2010)

Chapter 2 Microfabrication of FPAR

In this chapter the micromachining process to fabricate AlN based thin film acoustic resonators is described. The fabrication steps are similar to the FBAR technology and are presented here in the most generalized form.

When designing FPAR devices there are two aspects to be taken into account: how Lamb waves are excited and the way they are confined. When it comes to excitation there are two distinctive approaches: IDT concept and the longitudinal wave lateral field excitation (LW-LFE) transducers, in which the electric field is confined predominantly in the vertical direction, thus giving rise to lateral field excitation, employing longitudinal polarization through the e_{31} piezoelectric coefficient [1]. The LW-LFE transducer is represented by periodically aligned electrodes on top of the membrane and a continuous metal layer, covering the entire bottom surface of the membrane [2]. The process flow described here comprises both approaches, but the actual topology for a specific device will be discussed in the description of the corresponding paper in Chapter 4. The synthesis of AlN as the basic element of devices is also included together with a brief description of the electrical measurements of final devices.

The microstructures consist of a piezoelectric AlN thin film with thickness between 2 μm and 2.5 μm grown with preferentially (002) orientation, that is its crystallographic c-axis is oriented perpendicular to the surface, having Al as electrode (alternatively Mo or W as top electrode) and Ni as stop etch layer. In view of temperature compensation an additional layer of fused silica (SiO_2) is to be added (for details see Paper IV).

2.1 AlN Thin Film Synthesis

Aluminum nitride is a piezoelectric material of choice in high frequency thin film applications (FBAR, SMR, FPAR) due to its high acoustic velocity, high thermal conductivity, low dielectric and acoustic losses, moderate piezoelectricity, relatively low temperature coefficient of frequency (*TCF*) and moderate electromechanical coupling coefficient [3, 4, 5, 6], not to mention its IC compatibility.

Sputtering is a widely used method for depositing piezoelectric films, firstly, because it is part of the planar technology and secondly, it permits high-

volume manufacturing at low cost. In [7] interested readers can find details on basic principles involved in most deposition methods.

All AlN thin films employed in this thesis are grown using pulsed DC magnetron reactive sputter deposition. Systematic studies regarding the growth of highly textured AlN films have been performed by several researchers at Uppsala University [8].

The sputtering system used inhere is a conventional sputtering system Von Ardenne-CS 730. The AlN was deposited using a 4 inch Al target with a purity of 99.999% employing a balanced magnetron configuration. The base pressure was usually below 5×10^{-8} Torr. The gas mixture was Ar/N₂ with a flow ratio ranging between 24/36 and 26/34. Pulsed DC was applied at a discharge power of 900-1200 W. The substrate holder plate was at floating potential and no substrate heating was applied.

2.2 Microfabrication

All FPARs were fabricated on free-standing AlN membranes, using (100) 4-inch Si wafers as carrier substrates. After cleaning the substrate an Al thin film is sputter deposited, patterned using standard optical photolithography and etched in order to avoid parasitic capacitances (Fig. 2.1a).

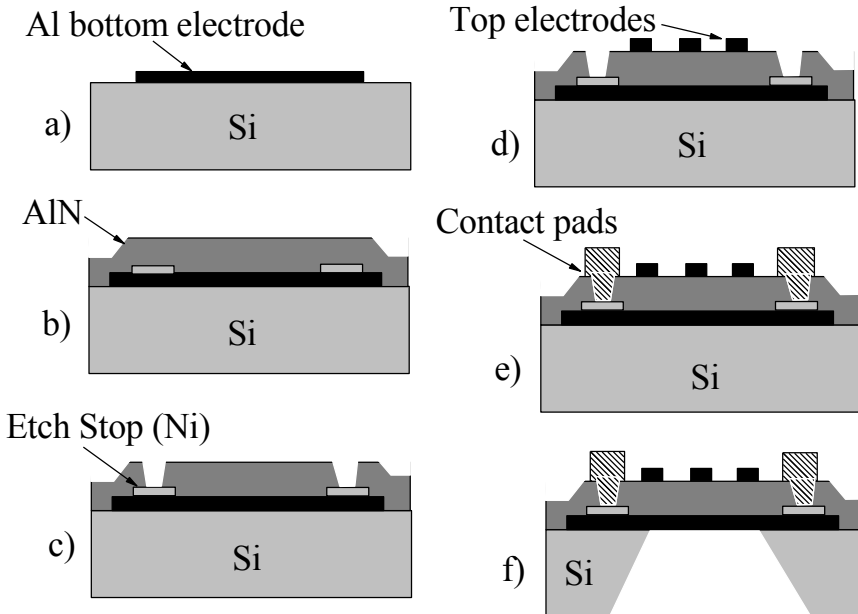
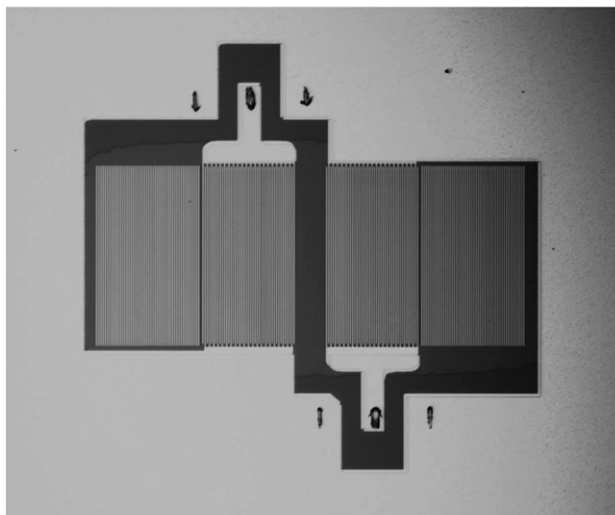


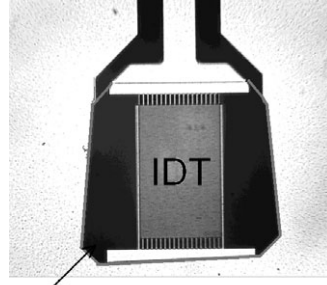
Figure 2.1 Generalized FPAR microfabrication scheme.

This can be done either by wet etching using standard commercial chemicals or by reactive ion etching (RIE) employing a $\text{Cl}_2/\text{BCl}_3/\text{O}_2/\text{Ar}$ gas mixture. After that a thin film of Ni is deposited to serve subsequently as an etch stop AlN film is deposited onto the bottom electrode using a Von Ardenne reactive balanced magnetron sputter deposition system operated in a direct current (DC) mode (Fig. 2.1b). Patterning of the Ni film is usually done with lift-off. Contact via-holes are patterned and etched by RIE, having as a mask a thick layer of photoresist or a hard Ni mask patterned with an Al mask (Fig. 2.1c). Another alternative is wet etching in hot ($\sim 40^\circ\text{C}$) solution of tetra-methyl-ammonium hydroxide (TMAH) using as mask a thin SiO_2 layer, but care should be taken in view of etch anisotropy. After creating the via-holes the top metal electrode (Al or Mo) is deposited, patterned and subsequently etched using RIE (Fig. 2.1d) to create the IDT and reflector grating, and at the same time to contact the bottom electrode. Since these devices are to be electrically characterized thick contact pads are also deposited (Fig. 2.1e), either by sputtering thick Al or by thermal evaporation of Ti/Al (Cu can be used as an alternative to Al and an additional Au layer can be evaporated). The former requires an additional SiO_2 or Ni layer to protect the structure while the latter employs the lift-off process. The last steps are related to the release of the membrane. First an Al film is sputtered on the backside of the wafer, patterned and subsequently etched using a wet chemical etch to form a hard mask. And finally, the last step is the deep Si etching by using a standard three step Bosch process (Fig. 2.1f).

In Fig. 2.2 are shown some pictures (top view) of microfabricated resonators.

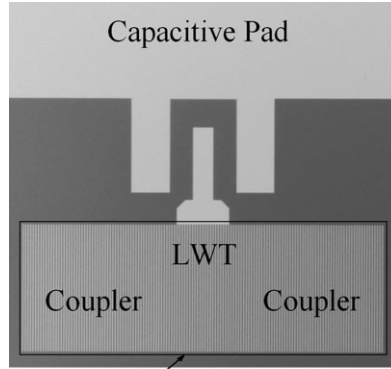


a)



Membrane

b)



Membrane

c)

Figure 2.2 FPAR devices as fabricated: a) 2-port FPAR, b) Zero Group Velocity Resonator (ZGVR), c) Intermode Coupled FPAR (IC-FPAR).

2.3 Electrical Measurement Set-Up

In this work a HP8364B vector network analyzer equipped with a G-S-G probe-station has been used to measure the S-parameters (scattering matrix) as function of frequency:

$$S = \begin{bmatrix} S_{11} & S_{12} \\ S_{21} & S_{22} \end{bmatrix} \quad (1)$$

For one-port resonators only parameters along the main diagonal of the scattering matrix (reflection coefficients) are different from zero. Thus S_{11} parameters, which are complex numbers represented by magnitude and phase (alternatively real and imaginary parts) have been measured while sweeping the frequency.

Before starting the measurement, the required calibration of the specific port has been performed for three standards: an open circuit, a short circuit, and a matched 50 Ohm load. The measured S_{11} parameters have subsequently been converted to admittance Z_{11} , alternatively impedance $Y_{11}=1/Z_{11}$, according to:

$$Z_{11} = Z_0 \frac{1 + S_{11}}{1 - S_{11}} \quad (2)$$

where $Z_0 = 50$ Ohm.

References to Chapter 2

1. J.F.Rosenbaum, Bulk acoustic Wave Theory and Devices, Norwood, MA: Artech House (1988)
2. V.Yantchev and I.Katardjiev, Micromachined thin film plate acoustic resonators utilizing the lowest order symmetric Lamb wave mode, *IEEE Trans. Ultrason. Ferroelectr. Freq. Control* **54**, 87–95 (2007)
3. K.Tominaga, T.Ao, I.Mori, K.Kusaka, T.Hanabusa, Gas Pressure Dependence of AlN Film Properties in Alternating Sputtering System, *Jpn. J. Appl. Phys.* **35**, 4972-4975 (1996)
4. H.Okano, Y.Takahashi, T.Tanaka, K.Shibata, S.Nakano, Preparation of *c*-Axis Oriented AlN Thin Films by Low-Temperature Reactive Sputtering, *Jpn. J. Appl. Phys.* **31**, 3446-3451 (1992)
5. K.Kusaka, T.Hanabusa, K.Tominaga, Effects of Nitrogen Gas Pressure on Residual Stress in AlN Films deposited by Planar Magnetron Sputtering System, *Thin Solid Films* **281–282**, 340-343 (1996)
6. S.Strite, M.E.Lin, H. Morkoç, Progress and prospects for GaN and the III–V nitride semiconductors, *Thin Solid Films* **231**, 197-210 (1993)
7. Thin Film Processes II Edited by: John L. Vossen, Werner Kern, 1991 Elsevier
8. G.Iriarte, F.Engelmark, and I.Katardjiev, Reactive sputter deposition of highly oriented AlN films at room temperature, *Mater. Res. Soc.*, **17**, 1469–1475 (2002)

Chapter 3 Acoustic Resonators Basic Characteristics

Frequency of operation f , effective electromechanical coupling coefficient k_{eff}^2 and quality factor Q are the most important parameters characterizing the performance of acoustic resonators and determine two descriptive *Figures of Merit* FOM: $Q \cdot f$ and $Q \cdot k_{eff}^2$ products respectively. In the present chapter k_{eff}^2 together with series and parallel resonant frequencies are defined through the Mason's one-dimensional model for a *free resonator*, that is a piezoelectric plate whose two faces are metalized [1, 2]. Despite the fact that this model is idealized it can be extended over real FBAR and FPAR configurations as well.

The quality factor Q is one of the most important parameters that characterize the resonator. There are different methods to determine Q [4]. Here two main approaches are presented: definition of Q at resonance and antiresonant [5] and Bode- or unloaded Q_B [6]. When comparing different resonator technologies it is important that the unloaded quality factor is accurately determined.

Further, for sensing application of resonators such parameters as noise, sensitivity and resolution are vital. High frequency sensors are thought to be superior when it comes to sensitivity, but this implies also lower quality factors resulting in higher noise. The main source of noise is the phase noise. It can be treated both in the frequency domain as signal power density and in the time domain as Allan deviation. Both approaches suggest that high Q and high input power are needed for high performance sensing. Further, the frequency stability with temperature is another important characteristic for frequency and time control applications (sensors, oscillators, filters).

3.1 Electromechanical Coupling Coefficient

In the Mason's one-dimensional model the resonator cavity is associated with an acoustic transmission line. The piezoelectric slab is bounded by stress-free boundary planes at $z_1 = d/2$ and $z_2 = -d/2$ having a thickness $d = z_1 - z_2$ in which an acoustic wave motion propagating along the vertical z -axis is induced (Fig. 3.1). The externally applied electric field coincides with the direc-

tion of wave propagation, also called *thickness excitation* (TE). (The case when the applied electric field is perpendicular to the direction of wave propagation is called *lateral field excitation* (LFE).) At each boundary inside the slab there are always two waves propagating in opposite directions: incident and reflected waves. The constructive interference of these two counter-propagating waves gives rise to the resonant behavior of the resonator.

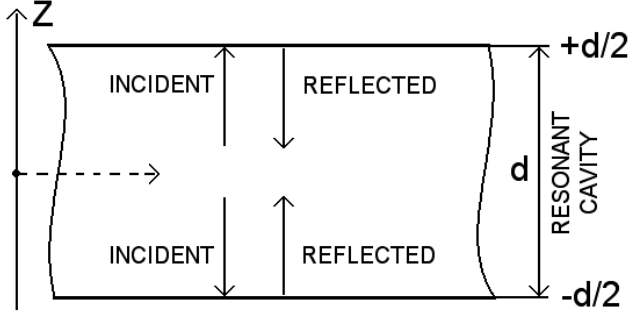


Figure 3.1 Schematic representation of excited waves inside a resonant cavity.

Thus the solution represents a superposition of plane waves travelling in forward and backward directions:

$$u = (a e^{-jkz} + b e^{jkz}) e^{j\omega t} \quad (3)$$

where u is the particle displacement, $\omega = 2\pi f$ and $k = \omega/V_{\text{wave}}$ are the angular frequency and wave number, respectively, and V_{wave} is the acoustic wave velocity. The particle displacements at each boundary, respectively, are:

$$\begin{aligned} u_1 &= (a e^{-jkd/2} + b e^{jkd/2}) e^{j\omega t} \\ u_2 &= (a e^{jkd/2} + b e^{-jkd/2}) e^{j\omega t} \end{aligned} \quad (4)$$

For the determination of the electrical impedance of the resonator piezoelectric constitutive equations for the stress and electrical displacement, written in one-dimensional form, are used:

$$T_3 = c_{33}^E S_3 - e_{33} E_3 \quad (5a)$$

$$D_3 = \epsilon_{33}^S E_3 + e_{33} S_3 \quad (5b)$$

Here T_3 is the mechanical stress, S_3 is the mechanical strain, E_3 is the electric field and D_3 is the electric displacement in the z -direction. The material constants c_{33}^E , e_{33} and ϵ_{33}^S are the stiffness constant, piezoelectric constant and the dielectric constant, respectively. Formula (5a) is defined when the electric

field is constant. At the same time the electric displacement \vec{D} should fulfill the Poisson's equation $Div(\vec{D}) = \rho_e$, where ρ_e is the density of free charges. But since for dielectrics there are no free charges in the bulk it means that $Div(\vec{D}) = 0$ and so the electric displacement is constant rather than the electric field. In fact, when only electro-acoustic waves are considered the electric displacement is zero since the polarizations caused by the elastic strain and the electric field cancel each other [1]. This fact makes the relation between mechanical stress induced by the wave and the acoustic wave strain, straightforward:

$$T_3 = \left[c_{33}^E + \frac{(e_{33})^2}{\epsilon_{33}} \right] S_3 = c_{33}^D S_3. \quad (6)$$

Here the parameter

$$c_{33}^D = c_{33}^E \left[1 + \frac{(e_{33})^2}{c_{33}^E \epsilon_{33}} \right] \quad (7)$$

is known as the stiffened elastic modulus and determines the acoustic wave velocity stiffened by the presence of piezoelectricity [1]: $V_{wave}^s = \sqrt{c_{33}^D / \rho}$, where ρ is the density of the medium. In eq. (7) $K^2 = (e_{33})^2 / c_{33}^E \epsilon_{33}$ is called the *piezoelectric coupling constant*.

At the boundary planes the total stress is zero since there is no external mechanical loading. Thus, combining the equation for the stress (5a), which equals zero at both surfaces, with the equations (4) and adding the applied external electric field the relation between the mechanical and electrical components of the field can be defined. After some routine algebraic manipulations the stress-free boundary condition becomes [1]:

$$\begin{aligned} \omega \frac{Z}{\sin(kd)} (u_1 - u_2) - \omega Z \tan\left(k \frac{d}{2}\right) u_1 + \frac{I(e_{33}/\epsilon_{33}^S)}{j \omega} &= 0 \\ \omega \frac{Z}{\sin(kd)} (u_1 - u_2) + \omega Z \tan\left(k \frac{d}{2}\right) u_2 + \frac{I(e_{33}/\epsilon_{33}^S)}{j \omega} &= 0 \end{aligned} \quad (8)$$

Here $I = j\omega A D_3$, is the displacement current, $Z = A\sqrt{c_{33}^D \rho}$ the acoustic impedance and A is the area of the resonator.

The total electric field has two components: external (from the applied voltage) and internal (electric field induced by the strain). It is noted that the electric displacement generated by the acoustic wave is zero:

$$E_3 = \frac{D_3^{ext}}{\epsilon_{33}^S} - \frac{e_{33}}{\epsilon_{33}^S} \frac{\partial u}{\partial z}. \quad (9)$$

Substituting this expression into the relation for the voltage $V = \int_{z_1}^{z_2} E_3 dz$ one can easily derive the following analytic expression for the current:

$$I = j\omega C_0 V - j\omega \left(\frac{e_{33}}{\varepsilon_{33}^S} \right) C_0 [u_1 - u_2]. \quad (10)$$

Here $C_0 = \frac{\varepsilon_{33}^S A}{d}$ is the static capacitance of the plate.

Solving equations (9) and (10) for the current and voltage one gets an expression for the electrical impedance of the resonator:

$$Z_{in} = \frac{V}{I} = \frac{1}{j\omega C_0} \left[1 - k_t^2 \frac{\tan(kd/2)}{kd/2} \right] \quad (11)$$

Here $k_t^2 = \frac{e_{33}^2 / \varepsilon_{33}^S}{c_{33}^D}$ is the *intrinsic electromechanical coupling coefficient* which is a measure of how much of the electric energy is transformed into mechanical energy of the elastic deformation. Theoretically k_t^2 is calculated by the expression:

$$k_t^2 = \frac{V_o^2 - V_m^2}{V_m^2} \quad (12)$$

where V_o and V_m are the acoustic wave velocities for a non-metalized and metalized surface, respectively. In the present thesis these velocities have been calculated using the Adler's approach [3].

Fig. 3.2 shows the frequency variation of the absolute value of the admittance $|Y| = 1/|Z_{in}|$.

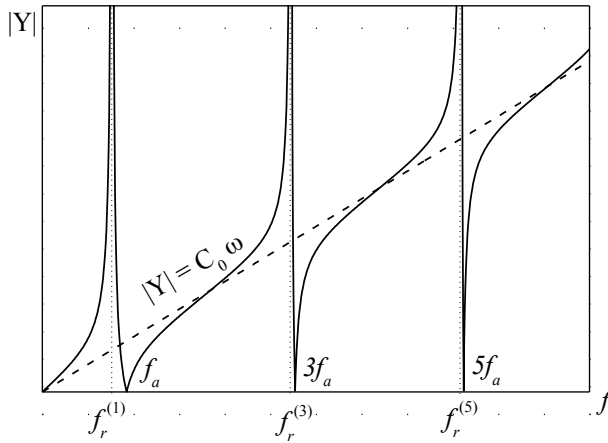


Figure 3.2 The frequency variation of the admittance of a free piezoelectric resonator. The straight line $|Y| = C_0 \omega$ is the admittance of the static capacitance C_0 .

The frequency at which impedance equals zero (the admittance is infinite) is called the resonance frequency f_r , while the frequency at which the impedance becomes infinite (the admittance is zero) is called antiresonance f_a , also known as series and parallel resonances, respectively. An approximate equation for the impedance can be derived by using the following expansion [7]:

$$\frac{\tan(kd/2)}{kd/2} = \sum_{N=1}^{\infty} \frac{8}{(N\pi)^2 - (kd)^2} \quad (13)$$

where $N=1, 3, 5, 7, \dots$ represents the harmonic of the operation. The poles (infinite impedance) of this function occur at $kd/2 = N\pi/2$. Taking into account the relationship between the wave number and frequency $k = 2\pi f/V_{wave}^S$ the antiresonant frequency is

$$f_a = \frac{V_{wave}^S N}{2d}. \quad (14)$$

The resonance is defined at $Z_{in} = 0$ and according to (11) $k_t^2 \frac{\tan(kd/2)}{kd/2} = 1$. Using the expansion from (13) the resonant frequency of the N th pole is:

$$f_r^{(N)} = \frac{V_{wave}^S}{2\pi d} \sqrt{(N\pi)^2 - 8k_t^2}. \quad (15)$$

Thus the electromechanical coupling can also be defined in terms of relative separation between both frequencies of the fundamental harmonic (for small couplings):

$$\frac{f_a - f_r}{f_a} \approx \frac{1}{2} \frac{f_a^2 - f_r^2}{f_a^2} = \frac{4k_t^2}{\pi^2} \quad (16)$$

or

$$k_t^2 \approx \frac{\pi^2}{4} \frac{f_a - f_r}{f_a}. \quad (17)$$

In real devices though neither impedance nor admittance is infinite. Thus the resonance is defined around the frequency where the impedance has a minimum (admittance has maximum) and its phase crosses zero with a negative slope while antiresonant occurs when the impedance has a maximum (admittance has a minimum) and the phase crosses zero with a positive slope, Fig. 3.3.

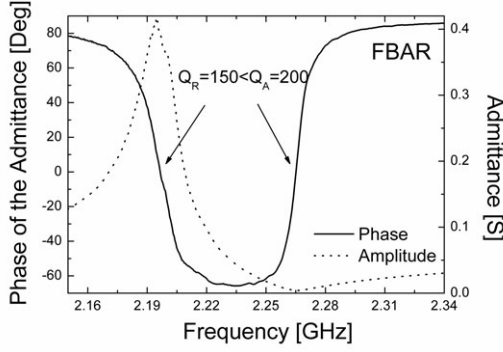


Figure 3.3 Magnitude and phase of admittance of a real FBAR.

Expression (17) can be employed for calculating the coupling coefficient by measuring the resonant and antiresonant frequencies of real resonators and is called *effective electromechanical coupling coefficient* k_{eff}^2 :

$$k_{eff}^2 = \frac{\pi^2 f_a - f_r}{4 f_a} \quad (18)$$

3.2 Quality Factor of a Resonator

As it was already mentioned, the quality factor Q is one of the most important quantities characterizing a resonator. Most generally, it is defined as the ratio between the stored energy and dissipated energy per wave cycle:

$$Q = \omega \frac{\text{Energy Stored}}{\text{Dissipated Power per one cycle}} \quad (19)$$

In other words it is a measure of the relative loss of energy in the resonator, which can have different origins: electrical, acoustic or dielectric.

In ideal resonators there are no losses therefore the Q factor is infinite. In real devices, however, Q is finite. For resonators of technological interest ($Q > 20$) the quality factor is usually extracted from the slope of the impedance (or admittance) phase curves Φ_Z (Φ_Y) at the resonance and antiresonance [4]:

$$Q_{r,a} = \frac{f_{r,a}}{2} \left| \frac{d\Phi_Z}{df} \right|_{f_{r,a}} \quad (20)$$

This definition of Q can be further used as an implicit indicator of resonance and antiresonance frequencies [8]. Thus, the series resonance is defined as the maximum Q near minimum impedance and the parallel resonance is defined as the condition of maximum Q near maximum impedance.

Generally, when connecting a resonator to an external circuit it affects its quality factor. That is why when comparing different resonator technologies it is important that the unloaded quality factor is accurately determined.

Based on a theorem derived by Bode [9] R. Ruby has developed an algorithm for attaining the unloaded Q of any real resonator by using the measured S_{11} reflection coefficients (scattering parameters) [6]:

$$Q_B = \omega \cdot \tau_{gd} \frac{|\Gamma|}{(1 - |\Gamma|^2)} \quad (21)$$

Here $\tau_{gd} = -d\varphi/d\omega$ is the measured group delay, φ and $|\Gamma|$ are the phase and the magnitude of the reflection coefficient. The procedure is the following: the S_{11} parameters are first measured in a 50 Ohm matched network, then using for example the ADS software to center the corresponding circle on the Smith Chart the new reflection coefficients are extracted. Equation (21) permits to determine the dependence of Q_B versus frequency.

3.3 Acoustic Resonators as Sensors

All acoustic wave resonators are sensitive to various biasing conditions caused by perturbations in different physical parameters: mass loading, ambient pressure, temperature drift, acceleration etc.

In acoustic wave sensors any perturbation along the path of the wave results in a change in the resonance frequency. The frequency change defines the sensitivity of a sensor. When designing a sensor, the minimum amount of change in the measured physical quantity that can be detected in the output signal (change in frequency) is desired to be as small as possible. In other terms, the signal-to-noise ratio (SNR) should be as high as possible. The sensitivity, generally, is rising with frequency, which together with decreased dimensions represent substantial benefits. Higher frequencies, however result in increased losses and hence phase noise, which, at best, results in moderate increase of the overall resolution. Thus, frequency stability together with sensitivity are of prime importance for high performance sensing.

In practice, resonators are devised as sensors by incorporating them into electrical circuits, for instance oscillators, where the resonator serves as the frequency-control element.

In oscillators, frequency stability is affected by temperature drift, long-term frequency drift (also called aging) and short-term instability. Aging effects are not part of this study. The effect of temperature on frequency is further described in Section 3.3.3 and the short-term stability of the oscillator frequency is represented by the term noise discussed below.

3.3.1 Noise in Frequency and Time Domain

An ideal oscillator produces a sinusoidal voltage at the output [10]. But even high Q oscillators are not ideal, and the amplitude and phase have random fluctuations. For this reason, the instantaneous output voltage of the oscillator can be described as a sinus function with modulated phase and amplitude:

$$V(t) = [V_0 + a(t)] \sin(2\pi f_0 t + \varphi(t)). \quad (22)$$

Here V_0 is the peak amplitude, f_0 is the mean or central frequency, t is time, $a(t)$ and $\varphi(t)$ are the time-dependent amplitude and phase *random* fluctuations, respectively. Well-designed oscillators have small or negligible amplitude fluctuations. Since frequency is the time derivative of the phase, the term $\varphi(t)$ describes equivalently the random frequency or phase fluctuations. The frequency at any instant t can be expressed as:

$$f(t) = f_0 + \Delta f(t), \quad (23)$$

where the deviation from the central frequency is

$$\Delta f(t) = \frac{1}{2\pi} \frac{\partial \varphi(t)}{\partial t}. \quad (24)$$

Phase noise performance of an oscillator is described in the frequency domain and the time domain using different terms. In the frequency-domain the frequency instability is measured by the power spectral density of the phase fluctuations $S\varphi(f_m)$ or the single sideband (SSB) phase density $\mathcal{L}(f_m)$, while in the time domain by the Allan variance $\sigma_y^2(\tau)$ or its square root Allan deviation $\sigma_y(\tau)$.

Phase Noise

In an ideal oscillator the signal power spectral density (measured in Watts per 1Hz of bandwidth) represents a single frequency spectral line. Further,

phase noise random fluctuations create continuous spectral sidebands above and below the nominal frequency f_0 , which decay rapidly with increasing frequency offset f_m (Fig. 3.4).

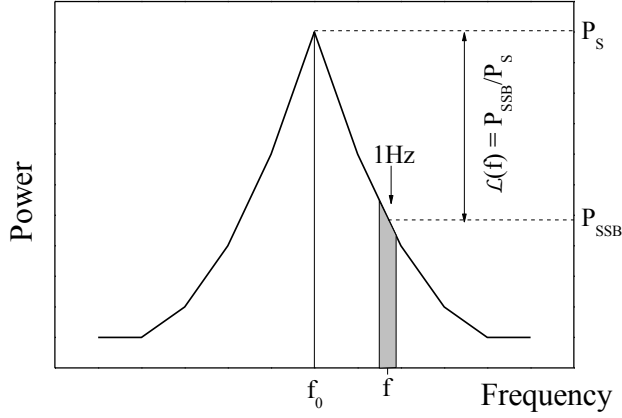


Figure 3.4 Spectral power distribution.

Single sideband, SSB, noise density is the power spectral density measured above the nominal frequency. This is a common form of describing the phase noise in the frequency domain [10]. The SSB noise density $\mathcal{L}(f_m) = S\varphi(f_m)/2$ is defined by the ratio (noise-to-signal):

$$\mathcal{L}(f_m) = \frac{\text{Power density in a single 1Hz sideband}}{\text{Total signal power}} \quad (25)$$

where $\mathcal{L}(f_m)$ is measured in dBc/Hz (decibels below the carrier in 1Hz bandwidth).

Generally, oscillators contain several active or passive components, with resonator and amplifier as basic elements, each one of them contributing to the phase and frequency fluctuations.

Before we look at the phase noise of an oscillator, let us take a look at the phase noise of the amplifier itself. For large enough offsets f_m the spectral power density of the phase fluctuations $S\varphi(f_m)$ of the amplifier is [11]:

$$S\varphi(f_m) = \frac{FkT}{P_s}. \quad (26)$$

Here F is the amplifier thermal noise factor, k is the Boltzman's constant, T is temperature in Kelvins and P_s is the signal power. Note that eq. (26) does not depend on frequency.

For $T=290\text{ K}$, $kT=4.00 \times 10^{-21}\text{ J}$, the above equation expressed in dB determines the thermal noise floor (TNF) of the amplifier [11]:

$$TNF = -174(dBm) + F(dB) - P_s. \quad (27)$$

When describing the noise of an oscillator the power-law was found to be a convenient model:

$$S\varphi(f_m) \propto f_m^\alpha, \quad (28)$$

where $\alpha = -4, -3, -2, -1, 0$. The thermal noise floor corresponds to $\alpha = 0$. Graphically, the dependence of the spectral power density $S\varphi(f_m)$ of phase fluctuations versus frequency is presented in Fig. 3.5.

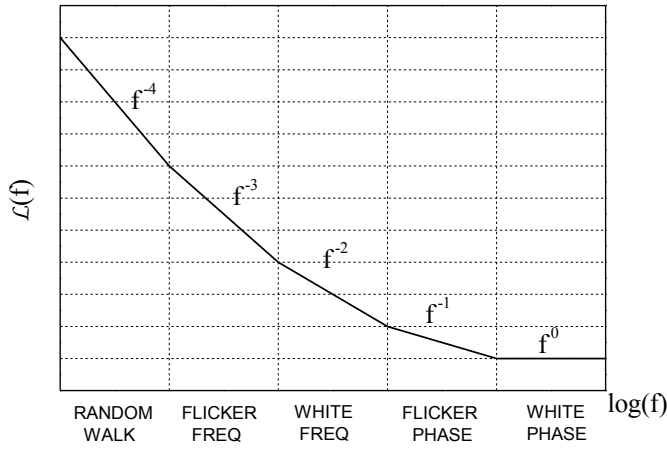


Figure 3.5 The spectral power density as a function of frequency offset.

D. B. Leeson summarized the SSB phase noise density $\mathcal{L}(f_m)$ of an oscillator as [12]:

$$\mathcal{L}(f_m) = 10 \log \left[\frac{1}{2} \left(\left(\frac{f_0}{2Q_l f_m} \right)^2 + 1 \right) \left(\frac{f_c}{f_m} + 1 \right) \left(\frac{FkT}{P_s} \right) \right]. \quad (29)$$

Equation (29) describes how the noise power density is distributed away from the main signal (Fig. 3.5). Each term in this equation has different origin. For example, the thermal noise floor, also called white phase noise, is mostly due to the sustaining amplifier, eq. (26). One way to minimize it is to increase the signal power. The resonator contributes to the $1/f^2$ (white frequency noise) as well as to $1/f^3$ (flicker frequency noise) terms [13]. The effect of frequency fluctuations of the resonator can be reduced by increasing its Q -factor.

Allan Deviation

In the time domain the standard for frequency stability measurement is described statistically in terms of Allan deviation also called two-sample deviation.

The instantaneous fractional frequency deviation is defined as, eq. (23):

$$y(t) = \frac{\Delta f(t)}{f_0}. \quad (30)$$

Measurement instruments do not provide instantaneous frequency values, but rather averaged values over a time τ starting from an instant t_i :

$$\overline{y_i(\tau)} = \frac{1}{\tau} \int_{t_i}^{t_i+\tau} y(t) dt, \quad (31)$$

where τ is the averaging time and $i = 1, \dots, N$ is a set of N measurements or samplings. Following a fundamental work of Allan [14], the IEEE has suggested a standard of measuring the Allan deviation [10]:

$$\sigma_y(\tau) = \sqrt{\frac{1}{2} \langle (\overline{y_{i+1}} - \overline{y_i})^2 \rangle} \quad (32)$$

here $\langle \dots \rangle$ denotes the infinite time averaging. In practice, however, the infinite time averaging is not possible and it is replaced by ordinary averaging over the number of measurements N :

$$\sigma_y(\tau) \cong \sqrt{\frac{1}{2(N-1)} \sum_{i=1}^{N-1} (\overline{y_{i+1}} - \overline{y_i})^2}. \quad (33)$$

As in the frequency domain, in the time domain phase noise is again described as a power-law:

$$\sigma_y(\tau) \propto \tau^\beta \quad (34)$$

where $\beta = -1, -1/2, 0, 1/2$. Graphically the Allan deviation is a plot of $\sigma_y(\tau)$ as function of the averaging time τ (Fig. 3.6):

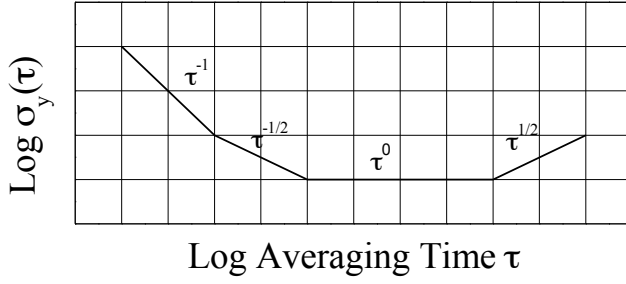


Figure 3.6 Allan deviation versus averaging time.

It is noted that in a certain interval the noise level is independent of the averaging time. The minimum achievable value $\sigma_y(\tau)_{min}$, which is nothing but the classical standard deviation σ_{std} , determines the noise floor of the oscillator. Typically it corresponds to averaging times between 0.1 and 10 s and contains noise, which cannot be eliminated by averaging. In the frequency domain, the τ^0 term corresponds to the $1/f^3$. As the sampling time further increases the Allan deviation starts to increase again due to the random walk noise related to the environment around the oscillator, like temperature, vibration, mechanical vibrations, etc.

More about possible phase noise sources can be found in [15].

3.3.2 Sensitivity and Resolution

In this section we look at how the noise influences the performance of a sensor. But first of all, to eliminate any confusion in terms, let us start with some basic definitions:

Sensitivity S of a sensor is the ratio of its response to the magnitude of the quantity measured (measurand).

Limit of Detection δ is the smallest detectable change in the measurand in the presence of noise.

Resolution R is the smallest detectable incremental change of input parameter that can be detected in the output signal.

According to the general definition of sensitivity:

$$S = \frac{\Delta f}{\Delta M} \quad (35)$$

where M denotes any physical quantity that is being measured, for instance mass, pressure or temperature, while ΔM represents the measure of its variation.

The sensitivity as defined in (35) scales with frequency. Quite common this dependence is a linear function, which in turn suggests the use of a normalized expression for sensitivity, thought to be a quantity with reduced sensitivity to frequency scaling:

$$S = \frac{\Delta f}{f_0} \frac{1}{\Delta M} \quad (36)$$

Further, a good estimation of the normalized minimum detectable frequency variation, or detection limit δ , is defined by three times noise floor:

$$\frac{\Delta f_{min}}{f_0} \equiv \delta = 3\sigma_y(\tau)_{min}. \quad (37)$$

Thus, the minimum change in the input parameter (ΔM_{min} here) that can be resolved or resolution R is the ratio between the three times noise floor and the normalized sensitivity (36) [16]:

$$R = \frac{3\sigma_y(\tau)_{min}}{S}. \quad (38)$$

According to [17] the empirical relationship between the smallest amount of noise generated by an oscillator in vacuum and the quality factor of the resonator is:

$$\sigma_y(\tau)_{min} = \frac{10^{-7}}{Q}. \quad (39)$$

On the other hand, the same authors [17] indicate that the maximum quality factor achievable is inversely proportional to the frequency, and for a specific material, crystal cut and mode of operation the following is valid:

$$Q_{max} \cdot f_0 = Const. \quad (40)$$

Therefore, the minimum noise, supposing that one can get the maximum Q , increases linearly with frequency:

$$\sigma_y(\tau)_{min} = Const \cdot f_0. \quad (41)$$

Thus the signal-to-noise ratio is determined by:

$$SNR = \frac{\Delta f}{\Delta f_{min}} = \frac{\Delta f}{f_0 3 \sigma_y(\tau)_{min}} \propto \frac{\Delta f}{f_0^2}. \quad (42)$$

Here the signal represents the change in frequency, and noise floor is determined by three times the Allan deviation.

Clearly, the resolution increases as the quality factor of the resonator increases. Correlating eq. (42) to the sensitivity scaling with frequency it appears that sensor resolution deteriorates with frequency scaling for linear function of absolute sensitivity versus frequency while for quadratic function (as for mass sensitivity [18]) it remains unaffected. A direct consequence of the eq. (38) is that resolution for temperature sensing of a given resonator deteriorates 10 times as the frequency improves 10 times – an observation discussed by J. Vig in [17].

This simple model suggests that the frequency scaling itself can hardly bring a sufficient improvement in sensor performance. The benefits of frequency scaling are to a large extent related to the reduced device size and the ability to integrate high performance small form factor devices in sensor arrays with miniature dimensions. Further, some device architectures enable sufficient improvements of the fQ product and relative sensitivity with frequency scaling, beyond the above presented simplified model, due to technological and design issues.

In conclusion, the design of high-resolution sensors requires a trade off between sensitivity and noise levels. In this context the FPAR approach proposed in this thesis can offer significantly increased sensitivities as compared to the widely explored SAW approaches, while keeping the noise levels comparable and even lower.

3.3.3 Thermal Stability

When operating at higher input powers the device temperature increases. It also changes due to variations in the environmental temperature.

The frequency stability as a function of temperature is described in terms of temperature coefficients of frequency (*TCF*). However, unlike the phase noise, which causes random in time frequency fluctuations, the temperature variation causes a frequency drift, which is constant for a given crystal cut and technology. Knowing these coefficients permits to design temperature-stabilized resonators.

The temperature dependence of the resonant frequency can be represented as a power-law series of the temperature variation [19]:

$$\frac{f(T) - f(T_0)}{f(T_0)} = \sum_{n=1}^3 TCF^{(n)} \cdot (T - T_0)^n \quad (43)$$

where T is the temperature variable and T_0 is the reference temperature. The coefficients

$$TCF^{(n)} = \frac{1}{n! f(T_0)} \left(\frac{\partial^n f}{\partial T^n} \right)_{T=T_0} \quad (44)$$

are the 1st, 2nd and 3rd order temperature coefficients of frequency.

The temperature drift of resonators relates to the changes in stiffness coefficients with temperature as well as to the thermal expansion, which affects not only the dimensions of the resonator, but also the density of the material [20]. Thus, most materials get “softer” with temperature and the acoustic wave velocity decreases, while others get “stiffer” and the velocity increases with increasing the temperature. The former have a negative first order TCF and the latter positive, according to the definition.

In practice, temperature compensation in devices can be achieved either by using material cuts with zero first order TCF (for example the ST-cut quartz) or by combining materials with opposite in sign TCF (for example, AlN has a negative TCF while SiO₂ - positive).

References to Chapter 3

1. J.F.Rosenbaum “Bulk acoustic Wave Theory and Devices”, Norwood, MA: Artech House (1988)
2. W.P.Mason, Piezoelectric Crystals and Their Applications to Ultrasonics. D. Van Nostrand, 1950
3. E.L.Adler, Matrix methods applied to acoustic waves in multilayers, *IEEE Trans. Ultrason. Ferroelectr. Freq. Control* **37**, 485–490 (1990)
4. D.Feld, R.Parker, R.Ruby, After 60 years: A New Formula for Computing Q is Warrented, *Ultrasonics Symposium* 2008 (Beijing)
5. K.Lakin, G.R.Kline, K.T.McCarron, High-Q Microwave Acoustic Resonators and Filters, *IEEE Transactions on microwave theory and techniques* **41** (12), 2139 (1993)
6. R.Ruby, R.Parker, D.Feld, Method of Extracting Unloaded Q Applied Across Different Resonator Technologies, *IEEE Intern. Ultras. Symposium* 1815 – 1818 (2008)
7. D.Royer, E.Dieulesaint, Elastic Waves in Solids II: Generation, acousto-optic interaction, applications, Springer-Verlag 2000

8. K.M.Lakin, G.R.Kline, R.S.Ketcham, A.R.Landin, W.A.Burkland, K.T.Mccarron, S.D.Braymen, and S.G.Burns, Thin Film Resonator Technology, *Proc. IEEE 41st Annual Frequency Control Symposium*, 371-381 (1987)
9. H.W.Bode, Network Analysis and Feedback Amplifier Design, Chapter 10, 196-225, Van Nostrand, New York 1945
10. IEEE Standard Definitions of Physical Quantities for Fundamental Frequency and Time Metrology—Random Instabilities, IEEE Std. 1139, Jul. 1999
11. R.W.Rhea, Oscillator design and computer simulation, Noble Publishing Corporation 2000
12. D.B.Leeson, A Simple Model of Feedback Oscillator Noise Spectrum, *IEEE Proceedings* **54**, 329-330 (1966)
13. E.Rubiola, V.Giordano, On the 1/f frequency noise in ultra-stable quartz oscillators," *Ultrasonics, Ferroelectrics and Frequency Control, IEEE Transactions* **54** (1), 15-22 (2007)
14. D.W.Allan, Statistics of Atomic Frequency Standards, *Proceedings of the IEEE* **54** (2) (1966)
15. D.A.Howe, D.W.Allan, and J.A.Barnes, Properties Of Signal Sources and Measurement Methods, *Proceedings of the 35th Annual Symposium on Frequency Control* (1981)
16. J.R.Vig, On acoustic sensor sensitivity, *Ultrasonics, Ferroelectrics and Frequency Control, IEEE Transactions* **38** (3), 311 (1991)
17. J.R.Vig, F.L.Walls, A review of sensor sensitivity and stability, *Frequency Control Symposium and Exhibition, 2000. Proceedings of the 2000 IEEE/EIA International* , 30-33 (2000)
18. H.Wohltjen, Mechanism of operation and design considerations for surface acoustic wave device vapor sensors, *Sensors and Actuators* **5** (4), 307-325 (1984)
19. R.Bechmann, A.D.Ballato, and T.J.Lukaszek, Higher-Order Temperature Coefficients of the Elastic Stiffnesses and Compliances of Alpha-Quartz, *Proceedings of IRE* **50** (8), 1812-1822 (1962)
20. J.H.Kuypers, Chih-Ming Lin, G.Vigevani, A.P.Pisano, Intrinsic temperature compensation of aluminum nitride Lamb wave resonators for multiple-frequency references, *IEEE International Frequency Control Symposium*, 240-249 (2008)

Chapter 4 Summary of Included Papers

4.1 Paper I “Thin Film Plate Acoustic Wave Resonators (FPAR): Part II”

(P1) Yantchev, V., Arapan, L., Katardjiev, I. (2009) Micromachined *IEEE Transactions On Ultrasonics Ferroelectrics and Frequency Control* 56(12): 2701-2710

This paper is a continuation of a previously reported work on thin-film plate acoustic wave resonators (FPAR) using the lowest order symmetric Lamb wave S_0 propagating in highly textured AlN membranes (Yantchev and Katardjiev 2007 *IEEE Trans. Ultrason. Ferroelectr. Freq. Control* 54, 87–95). The physical characteristics that make the S_0 Lamb wave attractive for practical use as discussed in the introduction, is the possibility for employing simultaneously high velocity, weak dispersion, and moderate electromechanical couplings.

This work is an experimental study of the FPAR performance vs. a variety of design parameters, such as device aperture, grating reflectivity, and synchronization.

The basic geometry of one-port resonators is presented in Figure P1.1. The reflectors are formed by a quarter wavelength Al strips periodically aligned on the top of the membrane surface and placed symmetrically on either side at one wavelength distance from the IDT. The IDT and the reflecting gratings have an equal pitch $\Lambda = \lambda/2$ and a metallization ratio $m = a/\Lambda$ (a is the strip width).

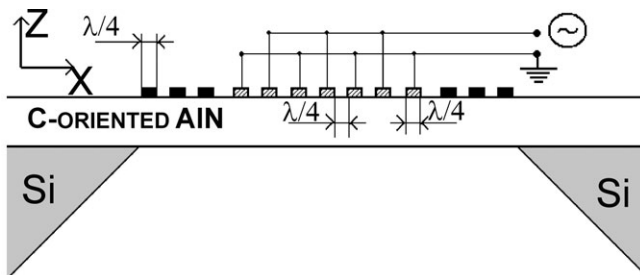


Figure P1.1 One-port Lamb wave resonator topology.

When propagating in membranes under infinite gratings, the S_0 mode exhibits a stopband behavior. In real devices, the gratings are of finite dimensions, and the number of strips is derived from the requirement for sufficient reflection. Generally, a resonator designed as in Figure P1.1 (synchronous design) operates in the vicinity of the upper frequency stopband edge.

It is demonstrated that the Q factor can be improved by a) adding more strips in the reflectors, b) improving the reflectivity of the grating (using thicker electrodes and also the possibility of using more reflective material is discussed) or c) increasing the device aperture. Another way to improve the Q factor is to design the resonator to operate inside the frequency stopband, where the reflection coefficient reaches its maximum. Thus, two different approaches have been identified. In the first approach, the IDT with regular electrodes is replaced by a split electrode transducer, having 3 electrodes per wavelength and the distance between the reflectors is shifted by a quarter wavelength from the synchronous regime (Figure P1.2).

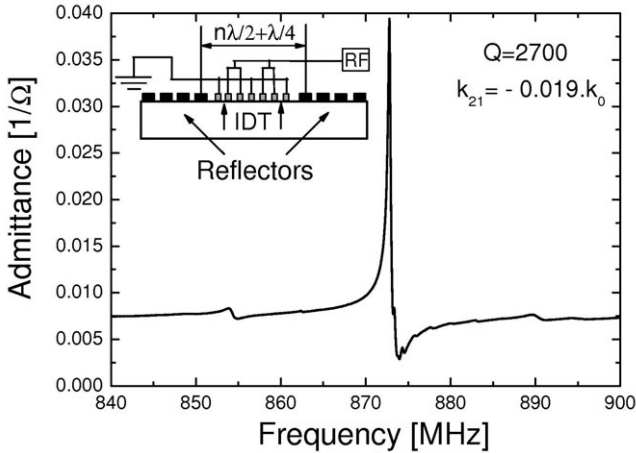


Figure P1.2 Close-to-resonance characteristics of 12- μ m wavelength FPARs operating in the vicinity of the stopband center: split electrode geometry.

The second design approach for in-band operation uses a quarter wavelength shift introduced inside the regular electrode IDT (hiccup geometry), while the reflectors are placed synchronously around the IDT (Figure P1.3).

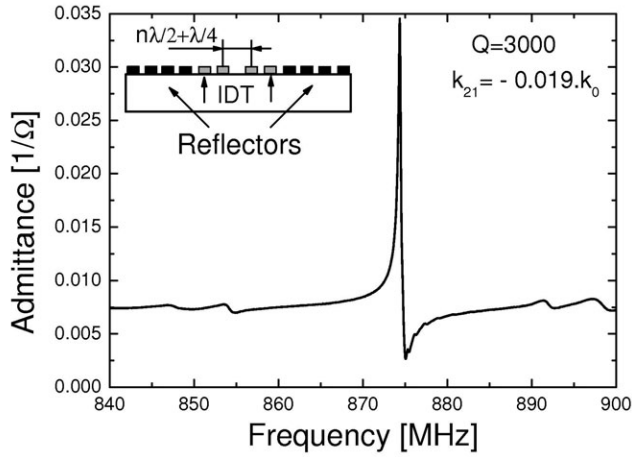


Figure P1.3 Close-to-resonance characteristics of a 12- μm wavelength FPAR operating in the vicinity of the stopband center: “hiccups” geometry.

It is noted that the latter approach is more advantageous when higher frequencies of operation are pursued, because it enables the use of wider electrodes in the transducer and thus promotes lower parasitics in the structure. Further, the possibility of reducing the membrane size by replacing the IDT with the longitudinal wave LW-LFE transducer employing a lateral field excitation is discussed.

Next, two-port FPARs have been designed and manufactured. The basic topology of a 2-port thin FPAR is shown in Figure P1.4. Such FPARs are IC-compatible and can be used, for example, in low-noise integrated feedback loop oscillators or as integrated narrowband filters.

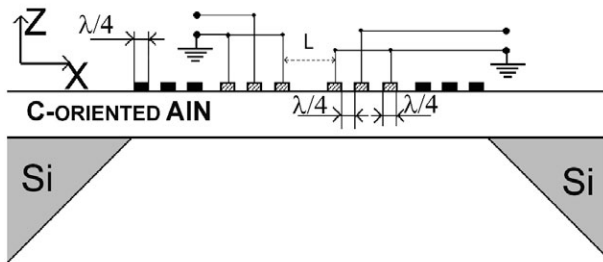
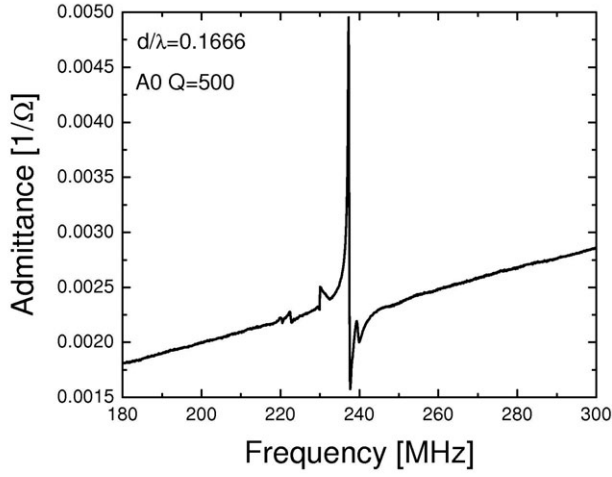
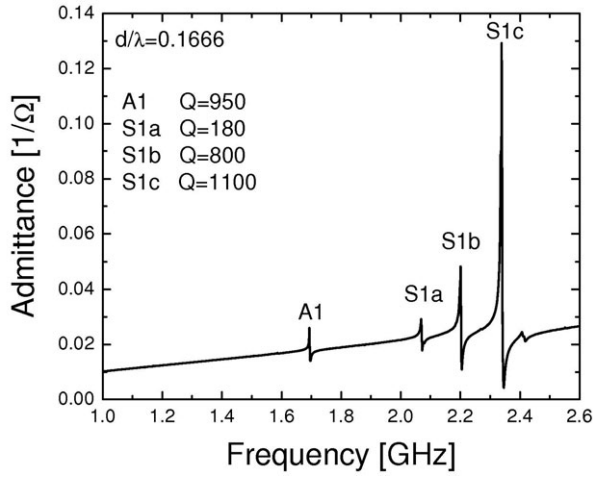


Figure P1.4 Two-port Lamb wave resonator topology.

Finally, from all FPAR devices studied, the identification of the different plate modes excited by means of IDTs was made by additionally investigating their dispersion characteristics. In Figure P1.5 the FPAR frequency spectrum is presented together with the measured quality factors for each mode. Additionally, the *TCF* for the corresponding modes have been experimentally determined for the first time.



(a)



(b)

Figure P1.5 FPAR frequency spectrum: (a) intermediate frequency and (b) lower GHz band.

Summarized Results

- One-port resonators using the lowest order symmetric Lamb wave demonstrated Q factors as high as 3000 at frequencies of around 880 MHz when operating at the center of the stopband.
- High Q, low-loss thin-film 2-port resonators using the S_0 plate wave have been demonstrated for the first time. Unloaded Q factors of around 3000 and insertion losses in the 5 dB to 8 dB range are demonstrated at frequencies around 890 MHz.
- The FPAR devices studied were used for the identification of the different plate modes excited by means of IDTs and the temperature co-

efficient of frequency for the modes in question experimentally measured.

- The properties of each observed mode are discussed in view of practical applications.

4.2 Paper II “A Micromachined Thermally Compensated Thin Film Lamb Wave Resonator for Frequency Control and Sensing Applications”

(P2) Wingqvist, G., Arapan, L., Yantchev, V., Katardjiev, I. (2009) *J. Micromech. Microeng.* 19(3): 035018

Thin film plate acoustic resonators utilizing the first order symmetric S_0 Lamb wave studied in Paper I as a high Q , low dispersion alternative to the high velocity SAW (HVSAW) in thin film based structures, can potentially be used for system-on-chip integration of frequency references and integrated circuits. In view of such applications, a notable drawback of the FPAR devices is the non-zero temperature coefficient of frequency. Thus, despite the promising features demonstrated, further device optimization is required. In this work zero TCF IC-compatible thin film resonators, utilizing the S_0 Lamb wave, are theoretically studied and experimentally verified.

A widely used technique for thermal compensation of AlN thin film based resonators is the addition of a compensating SiO_2 layer, since the two materials exhibit opposite TCF . The topology of the thermally compensated FPAR is presented in Figure P2.1, which resembles the topology of the FPAR presented in Paper I. Using Adler’s approach the propagation characteristics of the S_0 mode propagating in the AlN/ SiO_2 composite membrane were studied. The temperature coefficient of frequency was measured as a function of SiO_2 relative thickness for different AlN thicknesses. The analysis shows that the first-order TCF of Lamb waves on the AlN/ SiO_2 composite membranes has a dispersive character. In other words, the first-order TCF is a function of the relative SiO_2 thicknesses for different AlN thicknesses.

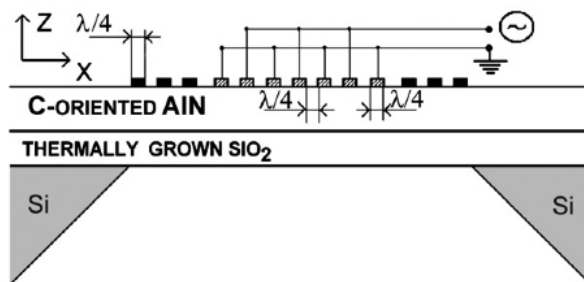


Figure P2.1 Topology of the thermally compensated FPAR.

The design parameters of the fabricated devices are presented in Table P2.1. For the design of the distributed reflectors the use of molybdenum (Mo) in the grating strips is employed owing to its high density and correspondingly high reflectivity.

Table P2.1 *Design parameters of the thermally compensated FPAR.*

AlN thickness	SiO ₂ thickness	Mo IDT thickness	Acoustic wavelength
2 μm	0.83 μm	270 nm	12 μm

In Paper I, two design approaches were identified: synchronous (operation in the vicinity of the upper stopband edge) and asynchronous with split electrode configuration (operation inside the frequency stopband). In this paper both designs are employed. Accordingly, detailed design parameters are shown in Table P2.2.

Table P2.2. *Design parameters (continuation).*

Type	Electrodes in IDT	Strips in reflectors	Device length	Aperture
Synchronous FPAR	79	53+53	1125 μm	500 μm
Asynchronous FPAR	50	32+32	680 μm	500 μm

To determine the TCF for each device, the devices were measured in the temperature interval from 25 to 90 $^{\circ}\text{C}$ and subsequently passively cooled down to 25 $^{\circ}\text{C}$ using a computer-controlled thermal chuck. The S_{11} parameters were then logged for each 5 $^{\circ}\text{C}$ step. The resonance frequency was extracted from the maximum of a mathematically performed curve fit to the real part of the impedance data; that is, the parallel resonance frequency was used since it is less sensitive towards probing than the series resonance.

The measurement results of the fabricated devices are listed in Table P2.3.

Table P2.3. *Device characterization.*

Synchronous FPAR			Asynchronous FPAR		
Q_s	Q_p	$k_{eff}^2, \%$	Q_s	Q_p	$k_{eff}^2, \%$
730	1410	0.65	1360	1310	0.33

The results show that asynchronous design has a lower effective coupling coefficient than the synchronous one, which is attributed to the split electrode configuration. The surprisingly low quality factor at series resonance for the synchronous design is explained by the etch rate inhomogeneity and the limited etch selectivity between Si and SiO₂ during the membrane formation step and in particular the aspect ratio dependence of the etch process. Thus, the larger membranes demonstrate Q factor degradation related to the non-uniformity of the membrane thickness.

The temperature coefficient of frequency for the non-compensated FPAR has been measured in the range -20 ppm/K to -25 ppm/K. Further, the experiment demonstrates temperature compensation in AlN/SiO₂ with relative thicknesses $d_{\text{AlN}}/\lambda = 0.1667$ and $h_{\text{SiO}_2}/\lambda = 0.07$, in agreement with theoretical calculations. Complete temperature compensation was observed at 40°C (turn-over temperature). At this temperature the first order TCF is zero and the second order coefficient dominates. From the relative resonance frequency shift versus relative temperature shift curve one can extract the second order TCF by making a fit with a quadratic polynomial function. Thus, at the turn-over temperature the second order TCF was found to be -31 ppb/K², which is higher than for the temperature compensated AlN FBARs (-20 ppb/K²), but lower than for SAWs on ST-cut quartz (-34 ppb/K²). It is noted that similar values have been obtained for both device configurations. These results are presented for comparison with the temperature compensated AlN plate wave resonators of edge-reflection type published subsequently (C.-M. Lin, T.-T. Yen, Y.-J. Lai, V. V. Felmetzger, M. A. Hopcroft, Jan H. Kuypers, A. P. Pisano, Temperature-Compensated Aluminum Nitride Lamb Wave Resonators, *IEEE Transactions on UFFC*, vol. 57(3), p. 524 (2010)) in Table P2.4. Comparison suggests that there is a trend of reduction in the 2nd order term as the composite membrane thickness to wavelength ratio become smaller. Thus, this effect can be further studied in order to cancel the 2nd order coefficient as well.

Table P2.4 Thermal compensation of the S_0 Lamb FPAR.

Type of FPAR	Resonance frequency, MHz	d_{AlN}/λ	h_{SiO_2}/λ	2 nd order TCF, ppb/K ²	Turn-over temperature, °C
Distributed reflectors	755	0.1667	0.07	-31	40
Edge-reflection	711	0.091	0.075	-21.5	18.05

Summarized Results

- Temperature compensation of thin film plate acoustic resonators utilizing the lowest order symmetric Lamb wave is theoretically studied and experimentally verified.
- Temperature-compensated low impedance 755 MHz FPARs having a second-order temperature coefficient of frequency – 31 ppb/K² and a Q factor of 1400 are successfully demonstrated.
- It is also found that temperature compensated asynchronous FPAR devices exhibit higher Q and smaller size in comparison with their synchronous counterparts.
- It is noted the possibility for further optimization with respect to minimizing the second-order temperature coefficient of frequency.

4.3 Paper III “Thin film plate acoustic resonators for integrated microwave power oscillator applications”

(P3) Arapan, L., Avramov, I., Yantchev, V. (2011) *Electronic Letters* 47(7): 453-454

In this Letter we report on two new features opening the way for FPAR technology into low noise integrated microwave oscillators. We show that FPAR devices can dissipate substantial amounts of RF-power without performance degradation and have very low residual flicker phase noise.

The 880 MHz FPAR devices we used in this study consist of two interdigital transducers and two reflector gratings to form a two-port resonator configuration as shown in Figure P1.4 (see Paper I). The acoustic wavelength is 8 μm and the AlN thickness is 2 μm . The typical measured close to resonance frequency response of the FPAR is shown in Figure P3.1. It has an insertion loss of about 5 dB and a loaded Q_L of about 700.

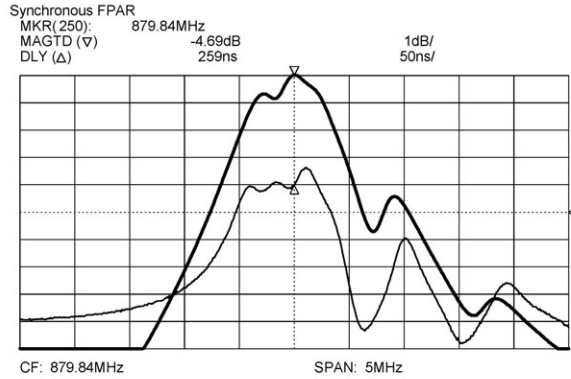


Figure P3.1 Close to resonance frequency response of the FPAR.

For the power measurements, the acoustic devices were then connected in a feedback oscillator loop, as shown in Figure P3.2, with a sustaining amplifier capable of dissipating 27 dBm (0.5 W) of RF power at the 880 MHz frequency.

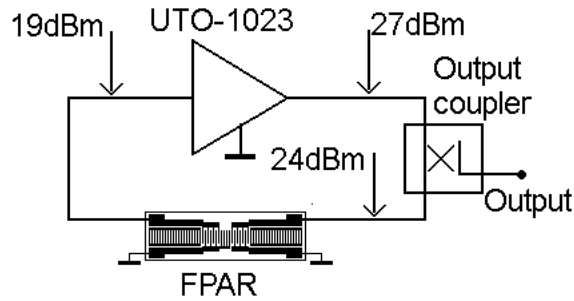


Figure P3.2 Block and level diagram of power oscillator loop.

In this power oscillator configuration the FPARs were operated at an incident power level of 24 dBm (250 mW) for five weeks. After that, the inspection of the device as well as the measurements showed no performance degradation, aging or metal migration. We expect that owing to the energy distribution in the entire free-standing AIN membrane, FPAR devices can handle even much higher than 24 dBm power levels before irreversible changes in electrical performance occur, if the sustaining amplifier could provide such power levels. For example, in SAW devices most of the energy is concentrated close to surface, thus SAW resonators running at this power level would fail within seconds.

Further, from the close-in phase noise measurements, the calculated flicker noise constant of the FPAR was found to be comparable with some of the best SAW resonators built to date in this frequency range and indicates the potential of FPAR technology for integrated low-noise oscillator applications.

The far from carrier phase noise of the oscillator determines the thermal noise floor (TNF). For this setup it was calculated to be -186 dBc/Hz. Such a low value is attributed to the high loop power that the FPAR can dissipate without performance degradation. At the same time the phase noise at 1kHz frequency offset was found to be - 92 dBc/Hz. For comparison, integrated Lamb wave based 1 GHz oscillators have shown a phase noise of -81 dBc/Hz at 1 kHz offset frequency and - 146 dBc/Hz for offset frequencies far enough from the carrier (C. Zuo, J. V. der Spiegel, G. Piazza, 1.05-GHz CMOS Oscillator Based on Lateral-Field-Excited Piezoelectric AlN Contour-Mode MEMS Resonators, *IEEE Transactions on Ultrasonics, Ferroelectrics, and Frequency Control*, **57** (1), 82-87 (2010)). Thus, they do not have a sufficient power handling capability to provide thermal noise levels below -175 dBc/Hz as required in high-performance integrated microwave clocks. At the same time, even if these two resonators have different topologies they show similar phase noise figures, indicating that the Lamb wave technology is a low noise one.

Summarized Results

- Two-port 880MHz FPAR devices operating on the lowest order fast symmetric Lamb wave mode (S_0) in c-oriented AlN membranes on Si, were fabricated and subsequently characterized in view of their power handling capabilities in a feedback-loop power oscillator circuit.
- Incident power levels of up to 24 dBm (250 mW) for the FPARs were provided by a high power sustaining amplifier in the loop. No measurable performance degradation was observed.
- The results from this study indicate that IC-compatible S_0 FPAR devices can dissipate orders of magnitude higher RF-power levels than their Rayleigh SAW counterparts on quartz and are well suited for integrated microwave power oscillators with feasible thermal noise floor levels of -180 dBc/Hz.

4.4 Paper IV “Sensitivity Features of Thin Film Plate Acoustic Wave Resonators”

(P4) Arapan, L., Anderas, E., Katardjiev, I., Yantchev, V. (2011) *IEEE Sensors Journal*, 11(12): 3330-3331

As already discussed, the S_0 mode provides some very attractive features, such as high propagation velocity, weak dispersion and moderate coupling coefficient. One-port FPARs have demonstrated Q factors of up to 3000 at a frequency of 0.9 GHz (Paper I) as well as robust thermal drift compensation (Paper II). Further, S_0 mode FPAR based oscillators have demonstrated phase

noise as low as -92 dBc/Hz at 1 kHz offset (Paper III). Here, we report on first tests aimed to assess the mass and pressure sensitivities as well as the possibility for in-liquid operation of the S_0 mode. These new features open the way for the FPAR technology into high-resolution integrated sensors.

The 0.9 GHz FPAR devices used in this study consist of an interdigital transducer and two reflector gratings to form a resonator as shown in Figure P1.1. Fabricated devices had Q factors of about 2000 and an effective coupling $k_{\text{eff}}^2 = 0.3\%$ at a resonant frequency of 886 MHz. The sensitivities of the FPAR were experimentally assessed through the relative series resonance frequency changes ($\Delta f/f_0$) caused by the presence of rigid mass, pressure and fluid.

Generally, the mass sensitivity can be assessed by relating the frequency shift to the density and acoustic thickness of the loading layer. Here the mass sensitivity towards SiO_2 layers for both the S_0 mode and the SAW at the same wavelength and AlN substrate has been theoretically calculated. Thus, the mass sensitivity of the S_0 mode was found to be about twice higher than the SAW and comparable to that of the FBAR.

In the subsequent experiments, the FPAR has been coated with low acoustic impedance SiO_2 thin films of various thicknesses h and the frequency response measured after each deposition step. Measurements not only proved to be in a good agreement with the theoretical expectations, but also showed that the device response and Q factor has not been affected by the layer deposition. This suggests that FPAR coated with glassy state sensing layers could offer high sensitivity in combination with high performance, which is a prerequisite for the development of high-resolution gas sensors.

The measurements on pressure sensitivity revealed sensitivity that is somewhat higher than for FBAR, reported in literature.

Finally, the in-liquid operation of the S_0 Lamb wave has been reported in literature employing a delay line topology. Here, the FPAR has been tested in contact with a liquid by dispensing a water droplet on the membrane backside. In Figure P4.1 the measured S_0 -mode FPAR responses are shown, demonstrating Q_s of 1700 (in air), 150 (in water) and 70 (in 50% glycerol water solution), respectively. It was observed a 9.2 MHz initial (from air to water) and additional 1.3 MHz (from water to 50% glycerol solution) frequency shifts, respectively.

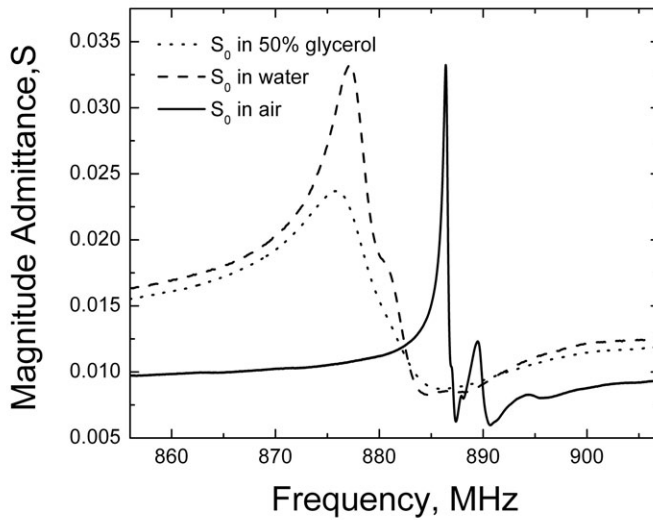


Figure 4.1 FPAR in-liquid operation.

Further, the improvement of the static capacitance due the dielectric permittivity of the water suggests that a FPAR design with bottom electrode would electrically isolate the FPAR from the liquid (making the device sensitive to the liquid mechanical properties only) as well as further improve the electro-mechanical coupling, resulting in better in-liquid performance.

Summarized Results

- The S_0 Lamb wave in thin film plate acoustic resonators has demonstrated high mass and pressure sensitivities.
- The ability to operate in liquid environment could be employed in integrated biosensor applications.

4.5 Paper V “Highly Mass-Sensitive Thin Film Plate Acoustic Resonators (FPAR)”

(P5) Arapan, L., Alexieva, G., Avramov, I. D., Radeva, E., Strashilov, V., Yantchev, V., Katardjiev, I. (2011) *Sensors* 11(7): 6942-6953

In this paper we study the mass sensitivity and the applicability of thin film plate acoustic resonators (FPAR), utilizing the S_0 Lamb mode propagating in thin AlN plates for gas sensing applications. When using an electroacoustic

device as an organic gas sensor, the device surface is coated with a sensitive layer that reacts selectively to the sorption of gas molecules, thus changing the resonance frequency.

The two-port FPAR devices used in this work have been presented in the Paper I. They have demonstrated an insertion loss of around 3 dB and an unloaded Q of 3000 at a frequency of 0.9 GHz. Also, 0.9 GHz FPAR based oscillators exhibited low phase noise (Paper III). These results, along with the expected high mass sensitivity of the S_0 Lamb mode (Paper IV), motivated us for the present study.

Theoretical Considerations

The mass sensitivity of the S_0 -Lamb wave in an acoustically thin plate loaded by a sensitive layer is described by using the equations of motion complemented by a full set of boundary conditions for a waveguided solution with polarization in the XZ-plane (see Figure P5.1). The S_0 solution consists of two guided modes representing the shear and the longitudinal polarization, respectively, in each layer of the composite plate. Subsequently, the equations of motion are applied to each layer of the composite plate along with the corresponding boundary conditions.

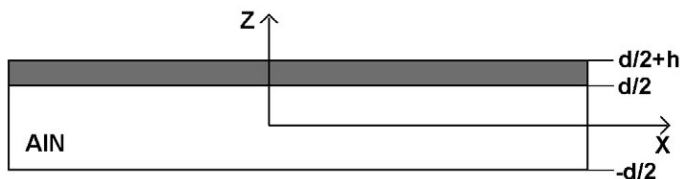


Figure P5.1 Geometry of the problem.

The mass sensitivity is assessed through the fractional variation of the acoustic velocity as a function of the sensitive layer thickness. For comparison, it is revealing to calculate theoretically the mass sensitivity of the S_0 Lamb wave and relate it to those of the Rayleigh SAW (RSAW) and Love wave propagating on layer coated AT-cut quartz, since gas sensors exploiting these waves have proved to have resolutions in the ppb range due to high sensitivity and very low noise levels.

In this specific case an AlN acoustic plate with a thickness-to-wavelength ratio $d_{\text{AlN}}/\lambda = 0.167$ as well as an AT-cut quartz substrate, both loaded with the glassy polymer (plasma polymerized) pp-HMDSO are theoretically studied. The calculated absolute fractional velocity shifts as a function of the pp-HMDSO relative thickness h_{HMDSO}/λ are shown in Figure P5.2.

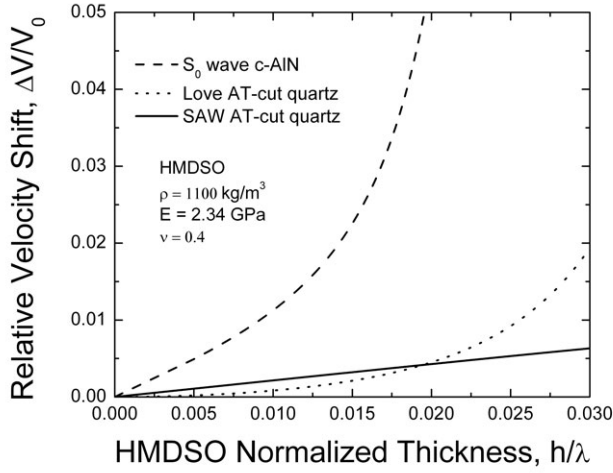


Figure P5.2 Theoretical mass sensitivity of RSAW, Love wave and S0 wave.

From this figure it can be clearly seen that the S0 Lamb mode has the highest mass sensitivity. However, increased sensitivity must not necessarily be the best choice for a practical system. Generally, improved mass sensitivity should correlate with improved damping (for example viscosity induced) especially at thicker layers. Otherwise, the increased attenuation and decreased device Q could result in serious degradation of the oscillator noise and sensor resolution. In Figure P5.3 the attenuation of the studied modes is shown as a function of the pp-HMDSO layer thickness in the presence of viscosity.

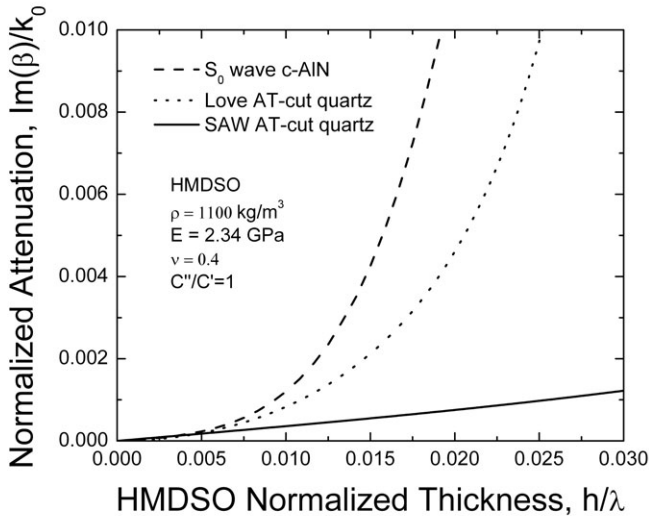


Figure P5.3 Attenuation of RSAW, Love and S0 waves. Here β is the complex wave number and k_0 - its real part.

On the other hand it was theoretically predicted that the viscosity itself tends to decrease the energy trapping in the low impedance layer, which in turn reduces significantly the sensitivity at thicker layers.

These results permit to conclude that the S_0 -Lamb wave in acoustically thin plates could demonstrate high sensor sensitivities obtained with relatively thin ($h/\lambda < 1\%$) glassy sensitive layers.

Experiment: FPAR mass loading with pp-HMDSO

We have compared theoretical relative frequency shifts of the S_0 -mode with experimental values. Experiments were performed with a 2-port FPAR with acoustic wavelength $\lambda = 12\ \mu\text{m}$ (grating pitch $6\ \mu\text{m}$). The FPAR device was micromachined on a freestanding AlN membrane with a thickness $d = 2\ \mu\text{m}$ resulting in a d/λ value of 0.1667. Then the FPAR was coated with hexamethyldisiloxane (HMDSO)-plasma-polymerized thin films of various thicknesses. In Figure P5.4 the experimental frequency shifts are compared to theoretically determined shifts assuming lossless pp-HMDSO film. For layer thicknesses $h/\lambda < 1\%$ the agreement between the lossless theory and experiment is excellent, while for thicker layers a progressive discrepancy is observed. The experimental data is seen to be in excellent agreement with the lossy theoretical predictions.

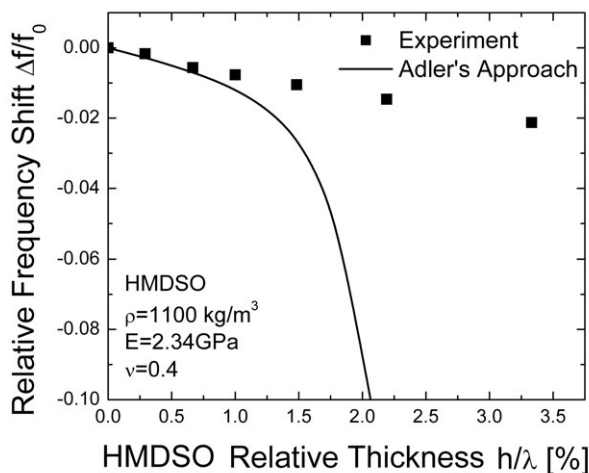


Figure P5.4 Theoretical versus experimental mass sensitivity.

Further, the recorded variations in the FPAR insertion loss as a function of the pp-HMDSO thickness showed relative losses of up to 2 dB for layer thicknesses $h/\lambda < 1\%$. For example, loading with 75nm pp-HMDSO layer caused a frequency downshift of 4600 ppm at the expense of just 0.6 dB induced losses. Moreover, FEM simulation suggested that FPAR devices coated with acousti-

cally thin pp-HMDSO could sustain high viscous losses before significant performance degradation occurs.

Experiment: gas sensitivity

We further considered a comparison of the FPAR gas sensitivity to that reported for other HMDSO-coated resonant devices using different types of acoustic modes (STW resonators at 700 MHz and SAW resonators at 430 MHz) versus xylene. The experimental sensitivity of the 380 nm HMDSO coated FPAR device to xylene concentration is shown in Figure P5.5. The sensitivity curve is nearly linear with a 31 Hz/ppm slope and the FPAR loss varied within 1 dB over the whole concentration range, which has a negligible effect on the sensor oscillator performance.

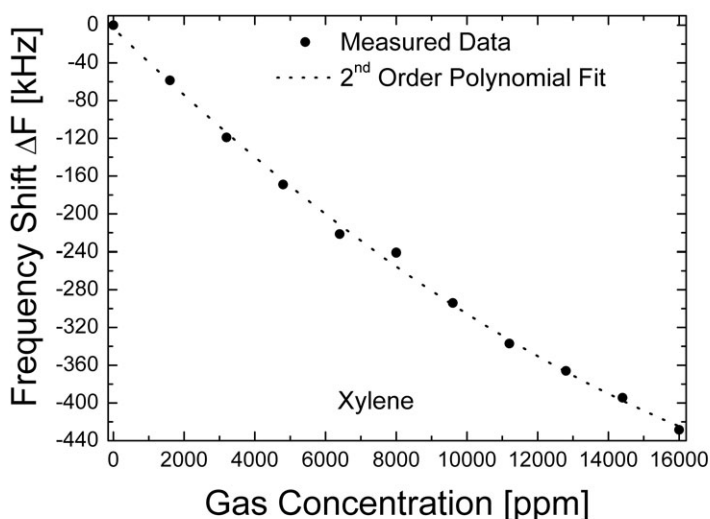


Figure P5.5 Sensitivity vs. xylene for the FPAR with 380 nm HMDSO.

This result is presented in a comparative manner in Table P5.1. Thus the relative sensitivities were found to be in relation 5.0/1.3/1.0 for FPAR vs. STW vs. SAW, respectively, which is in good agreement with the theoretical expectations.

These initial results from the gas sensing experiments clearly support the theoretical predictions for high mass-sensitivity of the studied resonator type. The considerable sensitivity improvement over one of the most efficient acoustic wave mode gas sensors—the STW, for the same types of polymer film and probing gas, and at comparable frequencies and losses, reveals the great potential of the S_0 mode for sensor applications.

Table P5.1. *Gas sensitivity vs different types of acoustic modes.*

	FPAR	STW	SAW
HMDSO relative thickness, %	3	1.4	3.9
Resonant Frequency, MHz	888	700	430
Sensitivity for Xylene, Hz/ppm	31	6.4	3.1

Further research is needed to explore the effects of membrane scaling on the sensor performance. The weak dispersion of the S_0 mode allows improving the sensitivity by decreasing the membrane thickness without any changes in the resonant frequency. This unique opportunity has also been discussed in contour-mode resonant configurations employing the same mode (G. Piazza, M. Rinaldi, C. Zuniga, Nanoscaled piezoelectric aluminum nitride contour-mode resonant sensors, in *Proceedings of IEEE Sensors Conference 2010*, Waikoloa, HI, USA, 1–4 November 2010; pp. 2202-2207). In this work a substantial improvement in sensitivity with increasing the frequency of operation and decreasing membrane thickness is demonstrated.

Generally, the improved sensitivity imposes stronger limitations on the gas sensitive coating thickness. Thus, the optimum FPAR sensor design is application specific, *i.e.*, requires a trade off between FPAR mass sensitivity and layer losses in order to achieve maximum resolution.

Summarized Results

- The mass sensitivity of thin film plate acoustic resonators has been experimentally and theoretically studied and more specifically the influence of the viscosity of the sensing layer has been studied. It has been found that the FPARs appear to exhibit specific advantages with respect to sensitivity and resolution under the condition that acoustically thin visco-elastic sensing layers are used.
- It has been proved that the symmetric Lamb mode used is considerably better in sensitivity compared to other acoustic modes such as SH-SAW or RSAW. As a result, in a gas sensing high frequency configuration the experimental relative sensitivity to a specific analyte has exhibited a 5-fold increase relative to other acoustic sensors.
- The findings highlight the potential of the FPAR in gas sensing applications in view of designing on-chip high-resolution sensor arrays for multiple gas detection.

4.6 Paper VI “Thin-film zero-group-velocity Lamb wave resonator”

(P6) Yantchev, V., Arapan, L., Katardjiev, I., Plessky, V. (2011) *Applied Physics Letters*, 99(3): 033505

Here we present a novel design of thin film plate acoustic resonators. It was previously noticed that the first symmetric S_1 Lamb mode can exhibit zero group velocity for a certain membrane thickness to wavelength ratio, that is $V_g = d\omega/dk$, which is related to the energy localization by definition. This could be beneficial for reducing the size and the complexity of devices since there is no need to use reflectors to confine the wave. In addition, it should be noted that the S_1 mode can be generated by means of IDT.

Design Considerations

To ensure that the S_1 mode from the metalized area of the resonator does not couple to the one from the area outside the metal electrodes, the Adler’s approach was employed to draw the respective dispersion curves (Figure P6.1). In this approach the active region is modeled as an AlN plate covered with an Al film. The Al thickness was taken as 3% from the AlN plate thickness. It can be seen that the group velocity is $V_g = 0$ for a membrane thickness-to wavelength ratio $d/\lambda = 0.3$ which corresponds to the lowest allowable frequency in the active area, $f_{D,A}$ and is lower than the lowest allowable frequency in the outside region, $f_{D,O}$. Thus the principle of energy trapping is satisfied. Accordingly the ZGVR inherently satisfies the above condition.

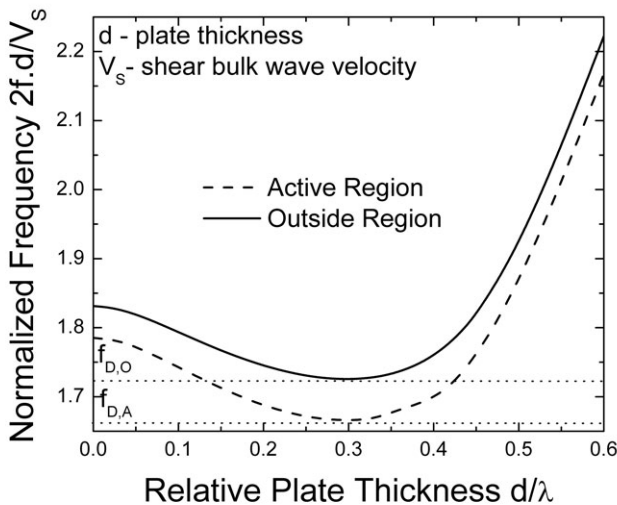


Figure P6.1 Dispersion curves of the S_1 mode under the IDT (active region) and in the outside region.

The topology of the fabricated devices is the one from the Figure P6.2. In this topology the condition for energy trapping is readily accomplished by the mass-loading effect of the electrodes.

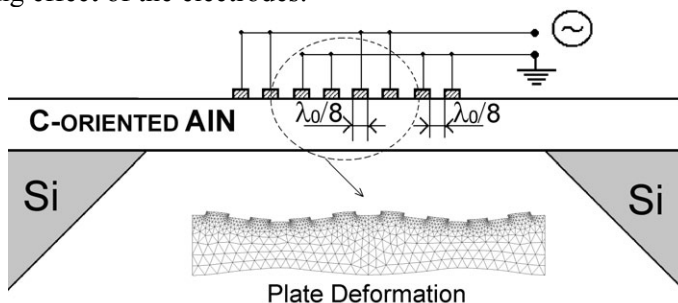


Figure P6.2 ZGVR device topology.

Experiment

Zero group velocity resonators were fabricated according to Chapter 2, but with some simplifications: no bottom electrode is present in the design and thus no via holes are needed.

In Figure P6.3 the measured wide span frequency response of the ZGVR admittance is presented. The ZGVR exhibit acoustic responses corresponding to the A_0 , S_0 and S_1 Lamb modes. Their phase velocities, $V = f \cdot \lambda_0$ are also included in the figure. It is noted that the only mode that exhibits a resonant behavior is the S_1 , since the IDT has a split-electrode topology to avoid confinement of other modes through internal reflection of the electrodes.

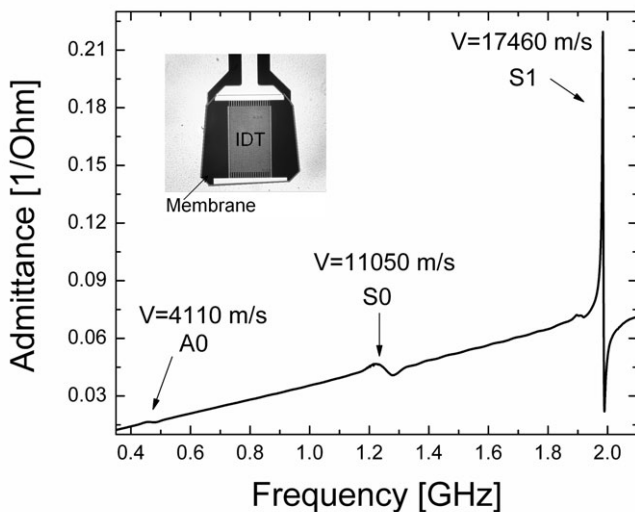


Figure P6.3 Wide-span frequency response.

Figure P6.4 shows the close-to-resonance frequency response of the ZGVR: magnitude and phase of the admittance.

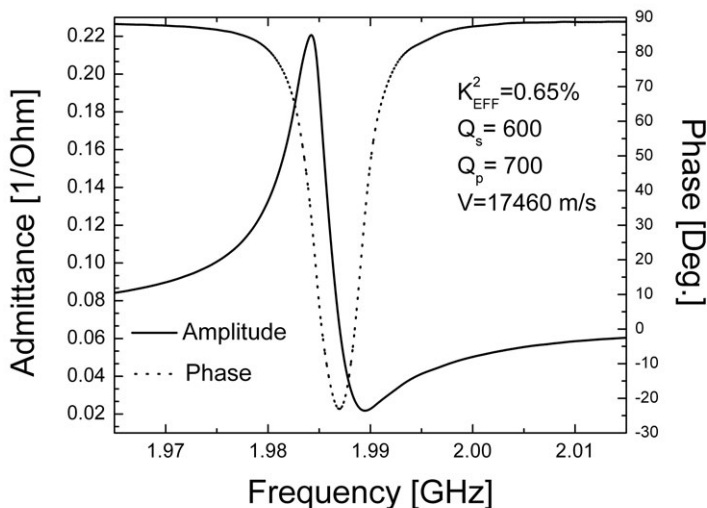


Figure P6.4 Close-to-resonance frequency response.

Summarized Results

- A concept for the development of thin film micro-acoustic resonators is demonstrated.
- The basic principles for the design and fabrication of zero-group-velocity Lamb acoustic wave resonators on c-textured thin AlN films are presented.
- The experimental results demonstrate that the zero-group-velocity waves can be employed in high frequency resonators with small form factors.

4.7 Paper VII “An intermode-coupled thin-film micro-acoustic resonator”

(P7) Arapan L., Katardjiev I., Yantchev V. (2012) J. Micromech. Microeng. 22(8): 085004

This work has been further selected for inclusion in the Institute of Physics’ selection “IOP Select” for its novelty, significance and potential impact on future research.

Here, we present a completely novel design approach employing efficient conversion between the S_0 Lamb wave and the fundamental thickness shear plate resonance in an attempt to combine the S_0 low dispersive nature with the

acoustic energy distribution of the fundamental bulk resonance. In this respect, the energy confinement will be promoted by means of grating couplers rather than reflectors. The concept presented here is thought to exhibit improved power handling capabilities compared to the classical Lamb wave resonator approach, while keeping the micro-fabrication robust.

Principles of operation

The conversion of the S_0 Lamb mode to the fundamental bulk shear resonance (that is the A_1 Lamb mode at its cutoff frequency) can be realized in structures with periodic gratings having the pitch equal to the S_0 wavelength.

According to Floquet-Bloch theorem a wave in a periodic structure can be represented by a superposition of an infinite set of discrete Floquet-harmonics $k_n = k_0 + 2\pi n/\Lambda$, that is, a fundamental harmonic with wave number k_0 and an infinite number of higher order harmonics $2\pi n/\Lambda$, where Λ is the periodicity of the structure. Thus, coupling between the A_1 mode and one of the S_0 Floquet-harmonics takes place when the pitch equals the central wavelength, $\Lambda = \lambda_0$. Further, this conversion is efficient when the frequencies of both modes coincide, imposing a strict relationship between the pitch Λ and the plate thickness d (since the parallel resonance of the fundamental shear bulk wave relates to the plate thickness as $f_{sh} = V_{sh}/2d$).

In the proposed device topology (Figure P7.1), the S_0 mode is excited using a longitudinal wave transducer employing a lateral field excitation principle (LW-LFE) via the e_{31} piezoelectric coefficient.

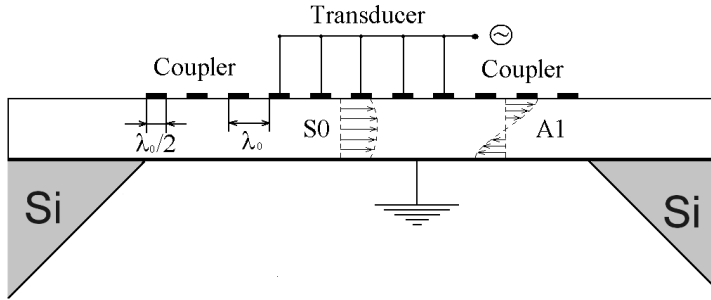


Figure P7.1 The IC-FPAR device topology.

The close to resonance dispersion curves for the specific design parameters are presented in the Figure P7.2, showing three fundamental stopbands. The largest stopband around central wavenumber is associated with an S_0 - A_1 interaction, with lower, upper and middle stopband edges (LE, UE and ME), respectively. In the middle of the stopband a strong non-propagating state comprising of a forward S_0 mode, a backward S_0 mode and a fundamental shear resonance is found to exist. Thus, a resonator designed to operate at the ME is expected to store part of its energy into the fundamental shear resonance due to the strong grating assisted intermode coupling.

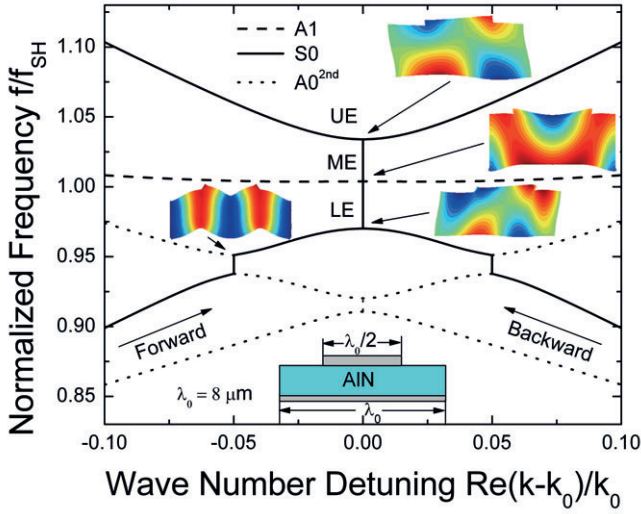


Figure P7.2 Dispersion characteristics.

Experiment

Microfabrication has been done according to Chapter 2. For the sake of simplicity, the bottom electrode has not been patterned and the via-holes in the AIN film have not been formed. Instead the excitation was realized through the capacitive coupling between the bottom electrode and large area thick metal pads.

Figure P7.3 shows the measured near resonance frequency response of the intermode coupled resonator admittance. In the same figure, a micrograph of the fabricated thin-film resonator is also shown. All three stopband edges are clearly identified and the main resonance occurs at the middle stopband edge, corresponding to the frequency of the fundamental shear bulk resonance.

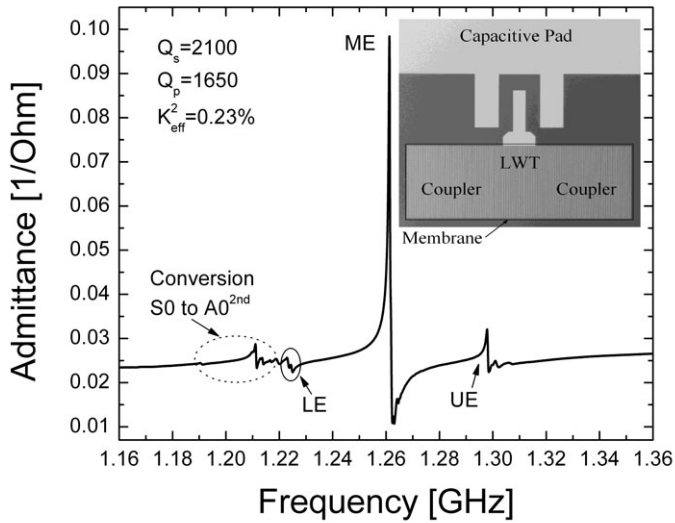


Figure P7.3 Close to resonance frequency response.

Summarized Results

- A novel concept for the development of thin-film micro-acoustic resonators based on the coupling between different plate acoustic modes was demonstrated.
- The basic principles for the design and fabrication of intermode-coupled plate acoustic wave resonators on c-textured thin AlN films were presented and first experimental proof of coupling between laterally propagating waves and BAW was demonstrated.
- The experimental results demonstrate that the grating-assisted intermode coupling can be employed in high-frequency resonators inheriting the low dispersive nature of the S_0 mode in combination with the energy localization in the plate bulk typical for the fundamental thickness shear resonance.

Summary and Discussion

Both, SAW and BAW technologies commercially available today, have their advantages as well as weak points. The surface acoustic wave technology distinguishes itself by its robustness, simplicity and low cost, but it is not IC compatible and is limited in terms of frequency of operation. On the other hand thin film bulk acoustic wave technology offer IC compatibility, high Q-factors, high power handling and high frequency of operation, though it is sensitive towards technological tolerances, which is crucial in high frequency range. More specifically, the frequency of operation of FBAR directly depends on the plate thickness. Thus, higher frequencies require thinner films and the film quality and thickness homogeneity is more than important.

Generally considered competitive these two technologies are rather complementing each other depending on the application. At the same time, both of them have reached their limits in terms of versatility. On the other hand FPAR, based on laterally propagating acoustic waves, enjoys the combination of robustness and simplicity of the SAW technology with the technological platform of FBARs, inheriting high power handling, high frequency of operation, high quality factors, but it is not sensitive to technological fluctuations since it employs the SAW principle of operation. In addition, it introduces versatility and new dimensions in EA.

This work was related to thin plate acoustic resonators operating on Lamb waves propagating in highly c-oriented AlN films. Its aim was two fold: i) to optimize the design of FPAR operating on the lowest order symmetrical Lamb mode and ii) to explore the possibility of designing resonators operating on other Lamb modes. In Paper I were presented one-port resonators demonstrating Q factors as high as 3000 at frequencies of around 880 MHz and for the first time two-port resonators exhibiting unloaded Q factors of around 3000 and insertion losses in the 5 dB to 8 dB range at frequencies around 890 MHz. However, a notable drawback of the demonstrated devices was the non-zero temperature coefficient of frequency. Thus, despite the promising features demonstrated, further device optimization was required. Accordingly, in Paper II temperature compensation of thin AlN film Lamb wave resonators was studied and experimentally demonstrated. Further, the results from Paper III indicated that two-port FPAR devices can dissipate orders of magnitude higher RF-power levels than their Rayleigh SAW counterparts on quartz and are well suited for integrated microwave power oscillators with thermal noise floor levels of -180 dBc/Hz feasible and phase noise at 1kHz frequency offset

of -92 dBc/Hz. In view of the obtained results, the possibility of IC integrated high performance small form factor sensors was discussed and the sensitivity of the S_0 Lamb was studied in Paper IV. This mode has demonstrated high mass and pressure sensitivities. In addition, the ability to operate in liquid environment could be employed in integrated biosensor applications. The mass sensitivity of thin film plate acoustic resonators has been experimentally and theoretically further studied in Paper V. It has been found that the FPARs appear to exhibit specific advantages with respect to sensitivity and resolution compared to RSAW and SH-SAW based resonators.

In the second part of the work, two new concepts for the development of thin film micro-acoustic resonators were demonstrated. In Paper VI the zero group velocity resonators (ZGVR), operating on the first symmetric (S_1) Lamb mode, which inherently exhibits zero group velocity for certain design parameters, were presented. The experimental results demonstrated that the zero-group-velocity waves can be employed in high frequency resonators with small form factors. In Paper VII the intermode-coupled thin film plate acoustic resonators (IC-FPAR) were designed and subsequently fabricated. The principle of operation is based on the coupling between different plate acoustic modes, specifically between laterally propagating waves (S_0) and BAW (fundamental shear resonance). Further optimization and research of these new types of resonators is required, in terms of quality factor, coupling coefficient, form factor, as well as temperature compensation, sensitivity, phase noise etc.

Svensk sammanfattning

Historiskt sett har forskningen inom detta område fokuserat på radartillämpningar för militära ändamål. Det grundläggande kravet på utformningen av sådana anordningar är hög prestanda med mindre fokus på pris och möjlighet till masstillverkning. Med övergången från militära till kommersiella tillämpningar, skiftade kraven drastiskt mot massproduktion till låg kostnad tillsammans med en acceptabel prestanda. Denna förskjutning har lett till en historisk övergång från resonatorer som nyttjar elektromagnetiska vågor till akustiska vågresonatorer. Dagens kommersiellt tillgängliga radiofrekvens-enheter (RF-enheter) är baserade på två konkurrerande tekniker, nämligen yt- och bulkakustiska vågresonatorer, dessa benämns SAW respektive BAW. Båda teknikerna använder piezoelektriska material och metallektroder för att omvandla elektrisk energi till mekanisk och vice versa, under nyttjandet av olika typer av elastiska vågor. Som namnet antyder, utnyttjar SAW-resonatorer akustiska ytvågor som utbreder sig på ytan av materialet medan BAW-resonatorer använda bulkakustiska vågor som utbreder sig i bulken. Jämfört med andra tillgängliga tekniker (dielektriska och vågledar-resonatorer), har vågbaserade resonatorer flera fördelar. Storleken på resonatorerna är normalt relaterad till våglängden, som i sin tur är direkt proportionell mot hastigheten och omvänt proportionell mot frekvensen, $\lambda = V/f$. Detta innebär att de akustiska resonatorer kan göras mycket mindre, givet samma driftsfrekvens, eftersom den akustiska våghastigheten är fyra till fem storleksordningar lägre än hastigheten på elektromagnetiska vågor. Både SAW- och BAW-resonatorer uppvisar höga godhetstal vilket resulterar i effektiv lagring och överföring av den akustiska vågenergin. Detta innefattar tunnfilmsdeponering, fotolitografi och tillverkningsbarhet på wafernivå. Den sista men inte minsta fördelen är att akustiska vågor lätt och enkelt kan exciteras och återomvandlas till elektriska signaler med hjälp av omvandlare tack vare den piezoelektriska egenskapen hos SAW- och BAW-material. Allt detta gör det möjligt att tillverka små, billiga och högpresterande enheter.

Övergången till enheter baserade på akustiska vågor har utlöst en exponentiell tillväxt på tillämpningar inom trådlös kommunikation (inklusive mobiltelefoner och bredbandstillämpningar) under de senaste 40 åren. Under 2006 översteg till exempel volymen av tillverkade SAW-filter 5 miljarder enheter. Generellt upptas den största delen av den trådlösa marknaden av SAW enheter eftersom det är en relativt mogen teknik och dess tillverkningsprocess är optimerad för att trycka ner priset till ett minimum. Tekniken är dock begränsad

vad gäller driftsfrekvens (upp till 2.5GHz) av tekniska skäl som kommer att diskuteras senare. En annan nackdel med SAW enheter är att de inte är kompatibla med integrerade kretsar (IC) grund av de material (enkristallina) som de syntetiseras på, vanligtvis SiO₂ (kvarts), LiTaO₃ (litiumtantalat) eller LiNbO₃ (litiumniobat). Å andra sidan har BAW-resonatorer använts inom elektroniken under många år, även innan SAW-tekniken var utvecklad, i synnerhet som kvartsresonatorer och fördröjningsledningar. Den övre frekvensgränsen för en typisk kvartskristall är dock begränsad av sin tjocklek. För att kunna använda samma driftsprincip i gigahertzområdet måste tjockleken på det piezoelektriska skiktet vara i storleksordningen mikrometer. Det enda sättet att bygga en sådan enhet är att använda tunnfilmsdeponering och metoder för mikrobearbetning. De resulterande enheterna är besläktade med tunnfilmsbaserade bulkakustiska resonatorer (FBAR) och fast monterade resonatorer (SMR), beroende på vilken metod som använts för att isolera den akustiska energin. Deras fundamentala nackdel är känslighet hos frekvensen för teknologiska variationer medan de samtidigt är IC-kompatibla (piezo-lagret är vanligtvis AlN deponerat på kisel) och har kapacitet att hantera hög effekt. Samtidigt har FBAR högre godhetstal på grund av mindre förluster jämfört med SAW-enheter.

Forskningen inom området elektro-akustik (EA) går kontinuerlig framåt. Som ett resultat av den senaste forskningen har en ny typ av akustiska resonatorer uppstått, tunnfilmsbaserad *plate*-akustisk resonator (FPAR), som nyttjar en annan typ av akustiska vågor, "Lamb"-vågor, som är kända som en typ av vågor som leds i plattor med fria gränser. Tillvägagångssättet med FPAR kombinerar funktionsprinciperna för SAW resonatorer med den tekniska plattform för FBAR enheter, vilket gör det möjligt att bygga enheter som har fördelar från både teknologierna: lätta att tillverka samt IC kompatibla med höga godhetstal vid höga driftsfrekvenser. Föreliggande arbete är en del av forskningen på tunnfilmsbaserade *plate*-resonatorer (FPAR) som har initierats vid Uppsala universitet vid avdelningen för fasta tillståndets elektronik omkring 2005 av Dr V. Yantchev. Arbetet i denna avhandling kan delas in i två huvuddelar:

1. En experimentell studie av de tunnfilmsbaserade *plate*-resonatorernas prestanda vid nyttjande av den lägsta symmetriska "Lamb"-vågen (S_0) som utbreder sig i mycket texturerade AlN membran utformade på en mängd olika sätt har utförts. Enheter som drivs i närheten av stopp-bandets centrum och som har ett godhetstal på upp till 3000 vid en frekvens runt 900 MHz har demonstrerats. Temperaturkompensering av denna typ av anordningar har studerats teoretiskt och realiserats experimentellt. Vidare uppvisade oscillatorer baserade på tvåportsresonatorer ett fasbrus på -92 dBc/Hz vid en offset på 1 kHz och möjlighet att få en lägsta nivå på det termiska bruset under -180 dBm/Hz korrelerat med förmågan att köras vid höga effektnivåer vilket manifesteras genom kontinuerlig drift i ett par veckor på nivåer för ingående effektnivåer på ca 24 dBm (250 mW) utan försämrade prestanda. S_0 -moden vi-

sade sig experimentellt vara mycket känslig för massa och tryck liksom lämplig för drift i vätska vilket tillsammans med lågt fasbrus och högt godhetstal gör den mycket lämplig för sensortillämpningar.

2. S_0 "Lamb"-moden är den mest exploaterade driftmoden i tunnfilmsbase-rade akustiska resonatorer. Den akustiska energin är avgränsad inom resonatorn genom reflektion från antingen en grupp av metallremsor (distribuerad reflektor) eller från de upphängda fria kanterna på membranet. I den andra delen av denna avhandling har forskningen inletts mot bakgrund av FPAR-enheter som nyttjar andra typer av "Lamb"-vågor som på ett innovativt sätt använder icke-reflekterande fysikaliska principer för att avgränsa energin inom resonatorn. I detta arbete har de första resultaten av design, tillverkning och karakterisering av två resonatorer av ny typ, ZGVR och IC-FPAR, base-rade på den första symmetriska S_1 respektive den första asymmetriska A_1 "Lamb"-moden förevisats. Båda nyttjar nya driftsprinciper. "Zero Group Velocity Resonator" (ZGVR) har utformats för att fungera vid ett visst förhållande mellan tjocklek och våglängd där S_1 "Lamb"-moden uppvisar noll gruppshastighet vilket i sin tur främjar inneboende självbegränsning av energin. "Intermode-Coupled FPAR" (IC-FPAR) använder brytningen av exciterade S_0 i A_1 moden och tillbaka genom en uppsättning av metallband som kallas gitterkopplare.

Acta Universitatis Upsaliensis

*Digital Comprehensive Summaries of Uppsala Dissertations
from the Faculty of Science and Technology 959*

Editor: The Dean of the Faculty of Science and Technology

A doctoral dissertation from the Faculty of Science and Technology, Uppsala University, is usually a summary of a number of papers. A few copies of the complete dissertation are kept at major Swedish research libraries, while the summary alone is distributed internationally through the series Digital Comprehensive Summaries of Uppsala Dissertations from the Faculty of Science and Technology.



ACTA
UNIVERSITATIS
UPSALIENSIS
UPPSALA
2012

Distribution: publications.uu.se
urn:nbn:se:uu:diva-178592